



Ultrasonic Imaging: Physics and Mechanism

1

Oliver D. Kripfgans and Hsun-Liang (Albert) Chan

1.1 Introduction

Ultrasound is a physical phenomenon with widespread use, including non-destructive testing and evaluation [1–3], cleaning [4], imaging [6–9], and therapy [10–18]. Medical ultrasound ranges from audio feedback only [19, 20] to 4D image sequences [21, 22] and comprises a multitude of specializations depending on the individual objectives. This section presents a brief overview of the mechanism of ultrasound. It explains how ultrasound is generated and what governs the propagation of ultrasound. The chapter also discusses ultrasonic exposure, i.e. the quantification of ultrasound with respect to safety and FDA regulations [21, 22]. Section 1.3 addresses ultrasonic imaging. This is the controlled transmission and reception of ultrasound in order to create diagnostic images. The concept of transducer arrays is introduced. Beamforming is explained with examples of steering and focusing of ultrasound beams. Spatial resolution is introduced and set in relation to physical quantities such as frequency, image depth, and aperture size. Penetration depth is explained and also placed in relation to user-controlled parameters such as transmit frequency. A number of basic and advanced imaging modes are introduced, and examples are provided. These include imaging anatomy and function. The latter is concerned with blood flow imaging in soft tissues. Advanced examples include harmonic imaging. While this mode was introduced for cardiac and liver imaging, it proves to be quite useful in dental imaging as

O. D. Kripfgans (✉)

Department of Radiology, Medical School, University of Michigan, Ann Arbor, MI, USA

e-mail: greentom@umich.edu

H.-L. (Albert) Chan

Department of Periodontics and Oral Medicine, School of Dentistry, University of Michigan, Ann Arbor, MI, USA

e-mail: hlchan@umich.edu

beam clutter is also seen when imaging the interdental papilla. The reader will also become acquainted with ultrasound scanner displays and ultrasound phantoms used to assess the performance of ultrasound systems and transducers. Section 1.4 closes this chapter with a discussion of imaging artifacts. These are important to know and recognize as ultrasound images frequently evince them. Real-time imaging allows the user to modify machine settings or transducer placement to avoid or minimize these artifacts.

1.2 Physics of Ultrasound

1.2.1 Generation of Ultrasound

A series of excellent textbooks positioned along a spectrum between solely physics and solely clinical are available [6, 9, 23–29].

This chapter is therefore meant as an abbreviated introduction to prepare the reader for the subsequent chapters of this book. The reader seeking an in-depth textbook on diagnostic ultrasound is referred to listed textbooks.

Sound is a mechanical wave and relies on the interaction of mechanical forces. In a loudspeaker, the speaker cone is pulsing in and out of the basket, mechanically driven by a coil. This coil in turn is driven by a magnet and the magnet by an electrical current. The entire system is thus converting electrical power into mechanical power and therefore electrical information into mechanical information. Again, in terms of audible sound, such as music from a radio, the electrical information of the music is converted into mechanical information, i.e. the sound. Ultrasound is exactly the same concept but at a frequency that is beyond the range audible to the human ear. This threshold is at 20 kHz. While some animals can hear and produce sound beyond 20 kHz, humans cannot. Current medical ultrasound for imaging is typically at even higher frequency, ranging approximately from 1 to 100 MHz. Figure 1.1 illustrates the concept of sound and ultrasound generation. Piezo crystals or similar materials are used to produce ultrasound. When a disc made from a piezo material is exposed to an electric potential, i.e. voltage, then the disc will either contract or expand in the direction of the voltage potential. In Fig. 1.1 this is illustrated on the right side by three scenarios. For negative voltage the crystal expands, for positive voltage the crystal contracts. In both cases, sound and ultrasound, loudspeaker and piezo crystal, an accelerated motion is required to produce (ultra-)sound. Were the loudspeaker cone or piezo-crystal to move linearly, no sound would be emitted. Figure 1.2 illustrates whether a moving surface can produce sound or not. In particular, four motion types are shown, i.e. two linear motions and two accelerated motions. Linear motion (panels a and c) does not produce a sound wave; accelerated motion (panels e and g), here a sinusoidal motion, does produce a sound wave. In medical ultrasound the displacement is typically a modulated sinusoidal function similar to rows four and five (panels e and f). Mathematically this can also be recognized by the wave equation. It describes how temporal changes in sound pressure p (left side of Eq. (1.1)) travel in space

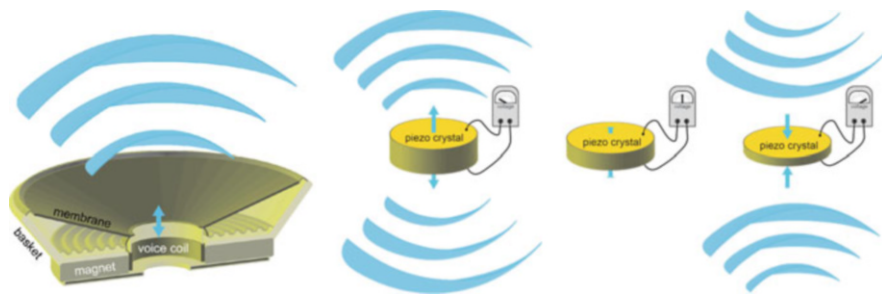


Fig. 1.1 Mechanics of generating sound and ultrasound. Left: Schematic of a loudspeaker illustrating how an electrical signal excites the magnet which then moves the cone to produce a (mechanical) sound wave. Right: Ultrasound can be generated by using a piezo crystal, whose thickness expands and contracts when exposed to negative or positive voltage, respectively (as indicated by the voltmeter)

(x) with sound speed c . A linear change has a zero second derivative and there is therefore no traveling pressure wave. Note that Eq. (1.1) is the most simplistic description of an ultrasound wave, it does not account for attenuation (absorption and scattering) nor diffraction or nonlinear effects.

$$\frac{\partial^2 p}{\partial t^2} = c^2 \frac{\partial^2 p}{\partial x^2} \quad (1.1)$$

The most common material to convert an electric signal into an acoustic wave is a piezoelectric crystal. Specialized piezoelectric composite materials have been developed from piezoelectric crystals to accommodate the unique needs of medical imaging, including efficiency and sensitivity of electrical-to-acoustic conversion. Figure 1.3 shows the composition of a typical ultrasound transducer. The expression *transducer* emphasizes the conversion of energy from one mode to another, i.e. here from electrical to mechanical. An incoming electrical signal causes the piezoelectric element to change its thickness and thus generate an acoustic wave, which then emerges on the front and back sides of the element. To eliminate the unwanted backside wave, an acoustic absorber is included in the housing. In addition, a backing block is placed on the rear side of the element. It is used to dampen the temporal extent of the piezo oscillation and dampen waves emerging from the back side of the crystal. Without this block, the piezo would continue to vibrate even after the electrical signal ceased and waves emerging from the rear of the crystal could ultimately interfere with the forward-traveling wave as well as received waves.

Piezoelectric materials differ significantly from human tissue in their mechanical/elastic composition. This difference causes acoustic waves to be reflected from human skin unless a *matching layer* is used. The matching layer is engineered to maximize the amount of acoustic energy that enters the human body when placed onto skin. Similarly audible waves traveling in air are reflected from rigid walls. In addition to the matching layer, there is a fixed-focus mechanical lens to focus

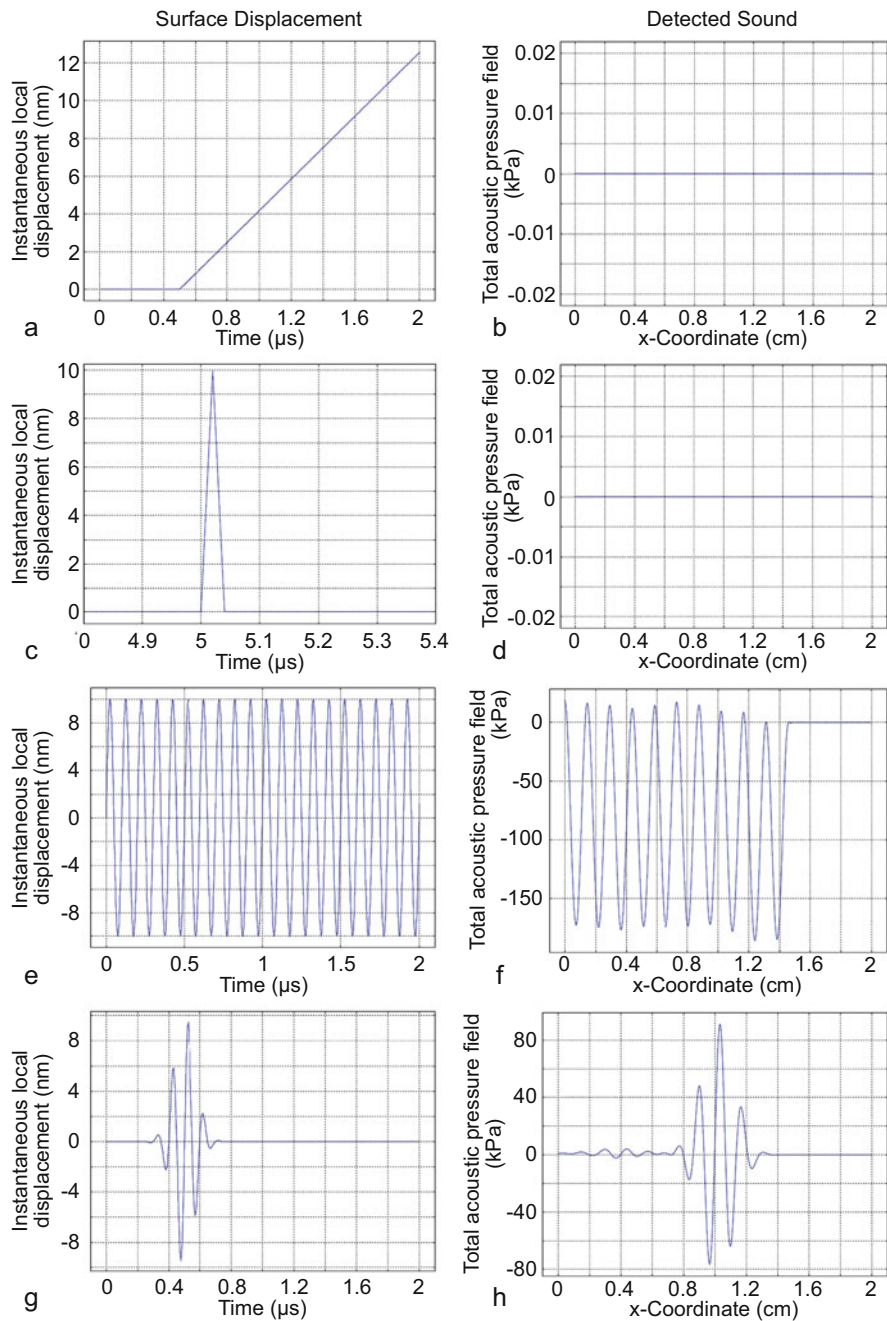


Fig. 1.2 Generation of sound and ultrasound. Left: Displacement of the sound-producing surface. Ordinate (x-axis) time in seconds, abscissa (y-axis) displacement in meters. Right: Resulting sound pressure. Ordinate space in centimeters, abscissa sound pressure in Pascals. First row: Linear

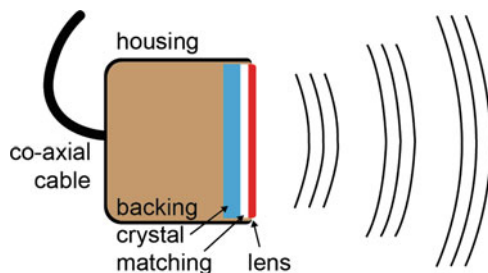


Fig. 1.3 Schematic overview of an ultrasound transducer. The piezoelectric crystal (element) generates a sound wave when driven by an alternating electric signal. It is encased by a matching layer in the front and a backing layer in the back. When placed in contact with human skin, sound travels through the matching layer into the soft tissue. Sound also travels through the backing block but is removed by the adjacent acoustic absorber

the generated sound at a specific distance from the transducer. Depending on the clinical use, a smaller or larger focal distance is desired. Vascular imaging typically demands a shallower focus than abdominal imaging, for example.

1.2.2 Propagation of Ultrasound

Ultrasound requires a medium to travel in. Medical ultrasound typically requires a medium similar to water. Human soft tissue has mechanical properties that are similar to water. Table 1.1 shows mechanical parameters significant for the propagation of an ultrasonic wave.

1.2.2.1 Speed of Sound

Speed of sound, as the name suggests, is the speed at which sound travels in the respective medium. Human soft tissue has a sound speed of approximately 1540 m/s; thus sound travels approximately 1.54 millimeters per microsecond. Ultrasonic imaging relies on timing. First the transducer emits an ultrasound wave (see Fig. 1.4) at which time a stopwatch is started. Any returning sound waves, i.e. those scattered by tissue structures or reflected from tissue boundaries, are recorded as a signal pair consisting of time and amplitude. The amplitude is a measure of how strong the scattering or reflecting structure is, and is depicted in the ultrasound

Fig. 1.2 (continued) displacement (monodirectional) of the surface after $0.5\ \mu\text{s}$, without resulting sound wave, since the displacement is linear. Second row: Also linear displacement (bidirectional), also without resulting sound wave. Third row, sinusoidal displacement with resulting sinusoidal pressure in the field. The field snapshot was taken after $10\ \mu\text{s}$, by which time the pressure wave had not yet arrived at the 1.5 cm x-coordinate. More about this effect is in Sect. 1.3.1. Fourth row, truncated sinusoidal pulse, also results in a truncated sinusoidal pressure wave. All data were produced by a one-dimensional finite element analysis using COMSOL Multiphysics™

Table 1.1 Acoustic properties relevant to the propagation of ultrasonic waves

Material	Speed of sound c [m/s]	Mass density ρ [kg/m ³]	Characteristic impedance Z [MRayl]	Attenuation coefficient α [dB/MHz ^{b} /cm]	b
Water	1489	1000	1.489	0.0021	2
Air	340	1	0.00034	40.5	2
Skin	1720	1093–1190	1.88–2.05	3.5 ± 1.2	–
Fat (subcutaneous)	1476	916	1.35	0.6	–
Muscle cardiac	1589–1603	1038–1056	1.65–1.69	0.24	1.04
Bone (cortical)	3850–4040	1990	7.66–8.04	4.34	–
Blood (whole)	1560	1060	1.65	0.12–0.16	1.19–1.23
Liver	1587	1050–1070	1.67–1.70	0.4	–
Gum	1540	1071	1.65	–	–
Tooth, cementum	3200	2090–2240	6.69–7.17	11.1	–
Tooth, dentine	4000	2030–2350	8.12–9.40	4.44	–

Note: Characteristic impedance is computed from c and ρ here [6, 30–36]

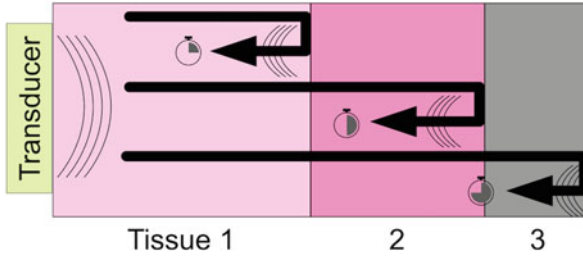


Fig. 1.4 Ultrasonic imaging relies on knowing the sound speed in the tissues imaged. Spatial information is derived from timing data. Received ultrasound signals are recorded as pairs of time and amplitude. By combining time and sound speed, the distance to the scattering or reflecting structure is computed and the recorded amplitude is displayed at that distance as a shade of gray. This is a simplified method by which an ultrasound image is generated

image by a gray scale. Light gray is a strong signal and dark gray is a weak signal. Time is used to determine where the reflection or scattering originated from and is computed as

$$s = c \cdot t \quad (1.2)$$

where s is the distance to the reflection or scattering structure, c is the speed of sound, and t is the elapsed time between the original transmission and when the signal was recorded. A structure at 1 cm depth is recorded at 20 mm divided by $1.54 \text{ mm}/\mu\text{s}$, i.e. $13 \mu\text{s}$. Since the sound has to travel to a depth of 1 cm, i.e. 10 mm, and return as well, the distance has to be doubled. Forgetting to double the travel path is a common mistake.

1.2.2.2 Acoustic Impedance

The product of speed of sound c and mass density ρ defines the characteristic acoustic impedance Z of a medium (Eq. 1.3). When ultrasound travels from medium 1 into medium 2 a certain fraction of sound pressure is reflected at the interface. This sound pressure fraction R is directly proportional to the difference in acoustic impedance between the two media and is defined in Eq. (1.3). The transmitted sound pressure fraction T is defined in relation to impedances Z_1 and Z_2 as well as R .

$$Z = c \cdot \rho$$

$$R = \frac{Z_2 - Z_1}{Z_2 + Z_1} \quad (1.3)$$

$$T = \frac{2Z_2}{Z_2 + Z_1}$$

$$T = 1 + R$$

Given Eq. (1.3) and acoustic properties from Table 1.1, sound propagating through soft tissue is reflected by bone at 60%. In addition, sound entering the bone will also be reflected at 60% when propagating back into soft tissue. Bone is therefore difficult to image in the frequency range discussed here (1–100 MHz). Dentine is comparable to cortical bone and reflects 66%. Sound propagation is inhibited when traveling between media with significant differences in their characteristic acoustic impedances. Small changes in the characteristic acoustic impedance between soft tissues, such as skin, fat, muscle, liver, and gum, result in small reflection coefficients and thus allow for excellent propagation.

1.2.2.3 Acoustic Attenuation

Acoustic waves are also diminished when traveling within a single medium. Acoustic absorption and scattering contribute to the acoustic amplitude attenuation coefficient α which is shown in Eq. (1.4). An acoustic wave with initial intensity I_0 is attenuated by $e^{-\alpha x}$ after traveling x centimeters within a medium with attenuation coefficient α . This is known as the Lambert–Beer Law. As the intensity diminishes exponentially, the attenuation coefficient is often provided in logarithmic units of decibel (dB).

$$I(x) = I_0 e^{-\alpha x} \quad (1.4)$$

The attenuation coefficient α is measured by comparing sound pressures or intensities before and after traveling inside the investigated medium. The natural computation of the attenuation coefficient is done by solving Eq. (1.4) for α . This leads to

$$\alpha_{Np} = \ln \left(\frac{I_0}{I(x)} \right) \quad (1.5)$$

The units of α_{Np} are called Neper, hence the subscript of Np . The relation of Neper to the above-mentioned unit of decibels, i.e. dB, is $8.686 = 20 \times \log_{10}(e^1)$. The definition of α in units of decibels and the relation of acoustic pressure amplitudes p to acoustic intensities $I \propto p_{rms}^2$ lead to therefore:

$$\begin{aligned} \alpha_{dB} &= 10 \log_{10} \left(\frac{I_0}{I(x)} \right) \\ \alpha_{dB} &= 20 \log_{10} \left(\frac{A_0}{A(x)} \right) \end{aligned} \quad (1.6)$$

Acoustic waves with higher frequencies are more attenuated than those with lower frequencies. A general description of the relationship between acoustic attenuation and frequency is given by Eq. (1.7). For a linear dependence of α to f , $b = 1$ and a

equals the constant acoustic attenuation defined above. In biological tissues b varies between 1 and 1.3 [30].

$$\alpha(f) = a \times f^b \quad (1.7)$$

As imaging frequencies range from 1 to 100 MHz, resulting attenuation can therefore vary significantly. A 10 MHz ultrasound wave traveling 1 cm through muscle loses 99.6% of its amplitude due to attenuation. Approximately $\frac{1}{5}$ of the attenuation is due to scattering, which is the signal used for imaging. Ultrasound scanners have a wide dynamic range to accommodate the reception of weak signals. Current electronics and signal processing allows for a 120 dB dynamic range and corresponds to 1:1,000,000, i.e. received signals can range from 1 V to 1 μ V.

1.2.3 Ultrasonic Exposure

Currently the FDA regulates two bioeffects of medical ultrasound [23, 24], namely cavitation effects and thermal effects. Those unfamiliar with cavitation may have seen pictures or video clips of ship propellers in water as they rapidly increase their rotating speed. Clouds of gas bubbles emerge around the propeller blades. They are produced by the blade surfaces that move away from the water. When the propeller turns, one side of each blade turns into the water, i.e. pushes the water in front of it away and the opposite side of the blade moves away from the water. That side is where the gas bubbles are created. When this side of the blade moves away from the water facing it, it creates a significant underpressure, as water tries to rush into the space that the blade leaves from. Figure 1.5 shows the generation of gas bubbles by a moving propeller as well as the resulting effects on the steel surface of the blades. While the forces in this example are much greater than those expected from diagnostic ultrasound, the underlying mechanism and the resulting effects are the same. The FDA regulates the mechanical and the thermal indices, i.e. the MI and TI, respectively. The MI is a measure for the likelihood of cavitation and is defined as the ratio of the acoustic wave peak negative pressure measured in MPa, divided by the square root of the center frequency of the acoustic wave (Eq. 1.8). An acoustic wave produces positive and negative pressures relative to the ambient static pressure. Figure 1.2, panel h, shows a pressure waveform similar to those from an ultrasound scanner. Its peak negative pressure is almost -80 kPa, whereas its peak positive pressure is 90 kPa. High-intensity waves show a larger amplitude discrepancy between the positive and negative pressures and the negative pressure causes cavitation, not the positive pressure. Per the FDA, the maximum safe MI in the absence of gas bodies in the field of view is 1.9. Examples of in situ gas bodies are gas pockets in the lung and in the intestine as well as any administered ultrasound contrast agent, which consists of microscopic gas bubbles. Ultrasound can also cause thermal effects, hence the TI. As mentioned above, acoustic attenuation is divided into scattering and absorption. The latter converts acoustic energy into heat. When same body part is scanned for a long time at highly repetitive acoustic

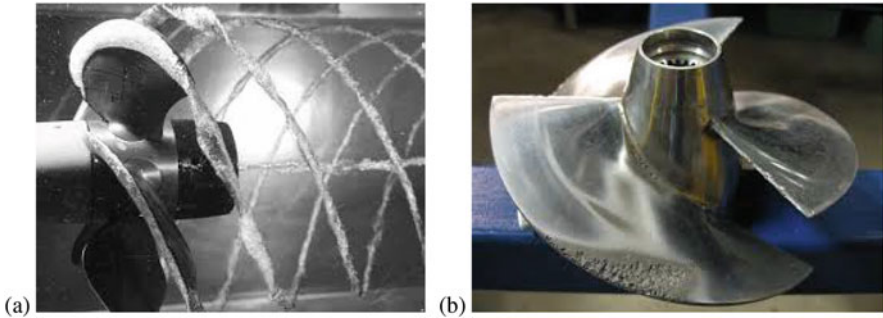


Fig. 1.5 Ship propellers are a classic example for cavitation. An example is shown in panel (a). The consequences of this effect are severe damage to the propeller blade as shown in panel (b). When cavitation bubbles collapse on the surface of the blade, they pinch the metal, and over time a substantial amount of the material is removed. In vivo, cavitation can destroy cells and can generate free radicals. That is why the FDA regulates acoustic output of ultrasound scanners to avoid unwanted cavitation in vivo. Copyright Wikimedia Commons (web pages: <https://images.app.goo.gl/wRSXxYRKS3N7aLok8>; <https://images.app.goo.gl/ixV5aJrzhmEtxup6>)

pulses, the temperature of that region will rise. A TI of 1 corresponds to the amount of energy W_p that raises the local temperature by 1°C (web page, 2019: <https://webstore.ansi.org/standards/nema/nemaud2004r20091358693>).

$$MI = \frac{p^- [\text{MPa}]}{\sqrt{f} [\text{MHz}]}$$

$$TI = \frac{W_p [\text{Nm/s}]}{W_{1^\circ\text{C}} [\text{Nm/s}]}$$
(1.8)

Safe use of ultrasound follows the ALARA (As Low As Reasonably Achievable) principle (web page, 2019: <https://www.aium.org/officialStatements/39>), which states that [ultrasound scanner] controls for acoustic output should be adjusted and transducer dwell times are minimized to reduce the risk of biological effects.

1.3 Imaging

1.3.1 The Concept of Beamforming

Ultrasonic images are generated by a technique called beamforming. As the name suggests, acoustic beams are generated, and images are created from these beams. This is not done by single piezoelectric elements but rather an array of these elements. The goal is to create images with large fields of view and sufficient spatial resolution depending on their ultimate clinical use. Beamforming is typically done for transmitting and for receiving a wave. Exceptions are discussed below.

1.3.1.1 Transducer Arrays

Imaging a two-dimensional region requires a one-dimensional ultrasound array of piezoelectric elements. A single piezoelectric element would only be able to determine the axial distance to the imaged object. By using a one-dimensional ultrasound array (1D array) geometric triangulation allows for differentiating objects in the lateral direction. This is achieved by steering and focusing the ultrasound beam in a desired direction and recording reflected and scattered signals. Transmitting and receiving ultrasonic signals is a symmetric process, i.e. the beamforming is equal, at least conceptually.

Transmit Beamforming Figure 1.6 shows simulations of transmitted ultrasound from an array of 16 elements. Four cases are shown. In the first case all elements are delayed by the same amount (panel (a)). The blue-colored sinusoidal signal symbolizes the electrical excitation of each piezoelectric array element (termed channel on the ordinate). The result is a planar wave front as seen in panel (b). Each array element emits a spherical wave (blue circles). The superposition of these spherical waves results in the planar wave front at 2 mm axial depth. In fact panel (a) shows the travel time needed for the wave front to reach the axial depth of 2 mm, i.e. $1.3 \mu\text{s}$, since ultrasound travels 1.54 millimeters per microsecond. For steering the planar wave front off-axis, a linear increasing delay must be added when exciting the array elements (panel (c)). An approximately $1 \mu\text{s}$ difference between the first and last element causes a 15° steered wave front. Focusing of the wave requires a complex delay that is approximately parabolic (panel (e)). The case shown focuses the wave at 2 mm axially, 0 mm laterally. When steering the beam also laterally, here to approximately 4.5 mm, an additional linear delay must be added (panel (g)).

Receive Beamforming When in receive mode, the ultrasound array records time-amplitude signal pairs for each element and stores this information for receive beamforming. If a strong reflection or scattered signal were to originate from an axial depth of 2 mm and lateral position of approximately 4.5 mm, then the recorded time-amplitude signal pairs would show strong amplitudes at specific times for each array element. These times are exactly the same as when focusing a transmit beam to the same location, which means that the specific times are the same as those shown in the bottom left graph of Fig. 1.6. Ultrasonic receive beamforming is therefore also called delay-and-sum beamforming.

1.3.1.2 Array Types

Ultrasound arrays are the acoustics analog to radio antennas. They transmit and receive (acoustic) waves and have specific design features. There are four common basic array types used in ultrasonic beamforming (see Fig. 1.7). A linear array is an assembly of typically 128 elements in one row spaced at the wavelength λ in the target medium, i.e. soft tissue. For a 10 MHz array and an average soft tissue speed of sound of 1540 m/s, the wavelength is $154 \mu\text{m}$ and thus a 128-element array is approximately 2 cm wide. To prevent mechanical cross-talk

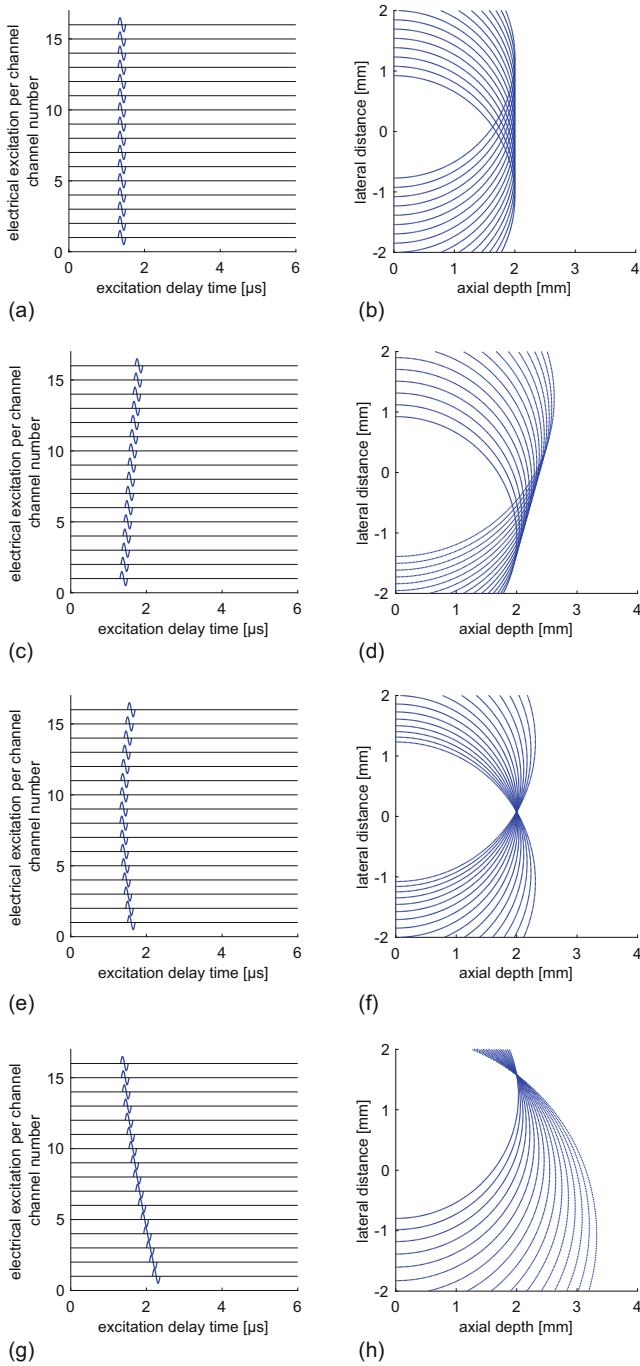


Fig. 1.6 Simulation of delayed transmission from a linear array of 16 elements. The left side graphs show the delay time in microseconds for each element. Simultaneous excitation of all

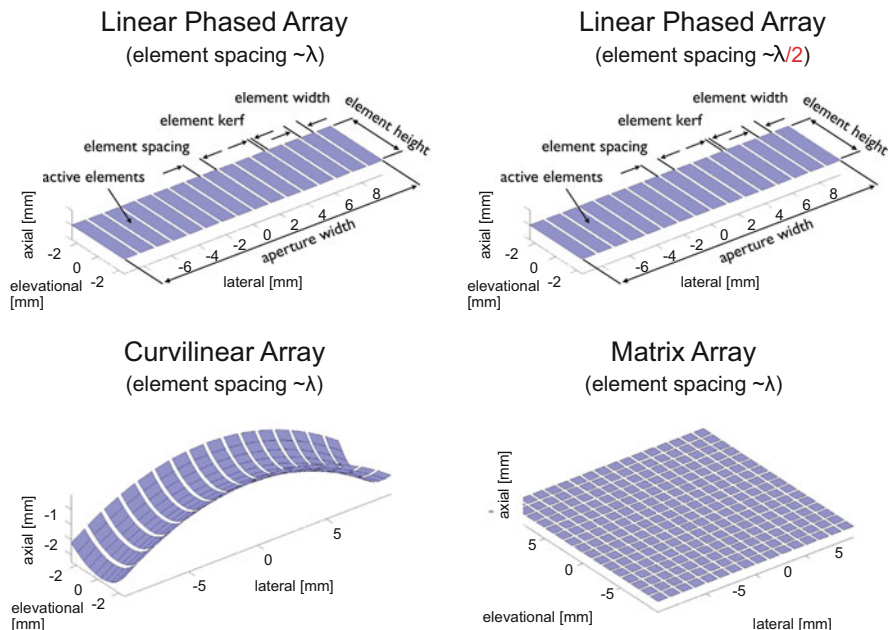


Fig. 1.7 From a beamforming point of view, there are four types of imaging arrays. The most common is the linear array (top left), whose elements are spaced at the wavelength λ . Element width equals the element spacing minus a trench between adjacent elements, termed kerf. Element height is multiples of the element width. Apertures are typically 128 or 192 elements wide and have a lens mounted in front of them to focus the beam in the elevational direction. This lens effect is illustrated in the bottom left panel (exaggerated curvature). For a larger field of view the array elements can be mounted in an arc shape in the lateral direction (bottom left panel). A phased array (top right) has all the features of a linear array, except that its elements are spaced by $\lambda/2$ (“2” intentionally in red). This feature allows for $\pm 90^\circ$ beam steering in lateral direction, whereas linear arrays can only steer $\pm 20^\circ$. Vector arrays (2D array, matrix array, bottom right) can steer beams in the axial and lateral directions and thus image a 3D volume. These arrays are expensive and require significantly more resources due to the large number of elements (2000–15,000). All graphics produced using Field II [5]

between adjacent elements a gap is placed between them, termed kerf. Element kerf may be approximately 10% of the element spacing. The emitted acoustic power is proportional to the radiating surface area. To achieve sufficient acoustic power the element height is therefore typically a multiple of the element width and a 10 MHz element may be several millimeters tall. While lateral focusing is achieved

←
Fig. 1.6 (continued) elements results in a planar wave front (panels (a) and (b)). Adding a linear delay between elements (panels (c) and (d)) results in a planar wave front that is steered. Focusing is achieved by delaying the excitation in an approximately parabolic fashion (panels (e) and (f)). To focus off-axis, a linear delay is added to the focus delays (panels (g) and (h))

by phase or excitation delays of the array elements, elevational focusing for a one-dimensional array relies on a fixed focus placed on top of the array elements. The focus of this lens depends on the intended application of the ultrasound probe. A small parts or peripheral vascular application benefits from a shallow focus ($\sim 2\text{--}3\text{ cm}$) and an abdominal or OB/Gyn application from a more distal focus ($\sim 10\text{--}15\text{ cm}$).

Curvilinear arrays are used in applications that require a large lateral field of view and provide a large acoustic window, i.e. allow for using a large aperture. The radius of curvature in the lateral direction depends on the lateral width of the aperture and is generally of the same order. For example, a 3 MHz abdominal probe ($510\text{ }\mu\text{m}$ wavelength) would be 65 mm wide and thus have a 65 mm radius of curvature. The above 10 MHz could have a much tighter 20 mm radius of curvature. Both arrays, linear and curvilinear, use variable fractions of the aperture, i.e. not all elements are always in use. Which elements are used depends on the imaging depth.

Phased arrays have all the features of linear arrays, except that the element spacing is only half the wavelength, i.e. $\lambda/2$. While a linear array can only steer $\pm 20^\circ$ in the lateral direction, a phased array can steer $\pm 90^\circ$, i.e. in the entire 2D image plane. This feature makes the phase array attractive for applications with small acoustic windows. Examples include liver and cardiac imaging, where the acoustic access is limited by the rib cage. Phased arrays always use the entire aperture, i.e. all elements.

Vector arrays have independent elements in the lateral and elevational directions, which requires up to 128×128 , i.e. 16,384 elements. Economically and technically this was a major barrier, if not prohibitive. While achieving a true two-dimensional array has the said barriers, arrays of various dimensions (D) have been developed. Table 1.2 lists fractional dimension arrays with their features and characteristics. A 1.25D array is essentially an array with an electronically adjustable aperture, which changes the elevational beam shape. Instead of one row of elements, there are 3, 5, or 7 rows. For a given application, these rows can be enabled or disabled. Typically more rows are enabled when imaging deeper and are symmetric to the main (middle) row. A 1.5D array consists of a limited number of elevational elements that can be individually amplitude-controlled but not delayed; thus elevational focusing can

Table 1.2 Features and characteristics of multidimensional ultrasonic arrays

Dimension (D)	Feature	Characteristics
1D	One row of elements	Classic linear or phased array
1.25D	Additional rows of elements (symmetric to main row)	Change elevational aperture size. No electronic elevational focusing or steering
1.5D	Limited 2D set of elements	Elevational electronic focusing, not steering
1.75D	No. of elevational elements \ll no. of lateral elements	Elevational electronic focusing, limited steering
2D	No. of elevational elements \sim no. of lateral elements	Full elevational electronic focusing and steering

be controlled, but there is no elevational steering. A 1.75D array possesses fully independent array elements with full amplitude and delay control in the lateral and elevational directions. However, there are fewer elements in the elevational direction than in the lateral direction. It is therefore possible to freely focus the beam in the lateral and elevational directions, allowing full steering in the lateral direction and limited steering in the elevational direction. A 2D array has none of these limitations.

1.3.2 1D, 2D, 3D Imaging

Conceptually, imaging is based on recording an electrical signal with timestamps and associating spatial locations to it using the speed of sound. A zero-dimensional imaging array, i.e. 1 element only, can resolve axial positions only. Figure 1.8a illustrates this scenario. A one-dimensional imaging array (b), i.e. a row of transmit/receive elements, can in addition provide lateral information and therefore create a two-dimensional image (Fig. 1.8b). The most sophisticated is a two-dimensional imaging array (c). It can provide triangulation in all three dimensions and thus deliver image volumes. The current standard is one-dimensional arrays for

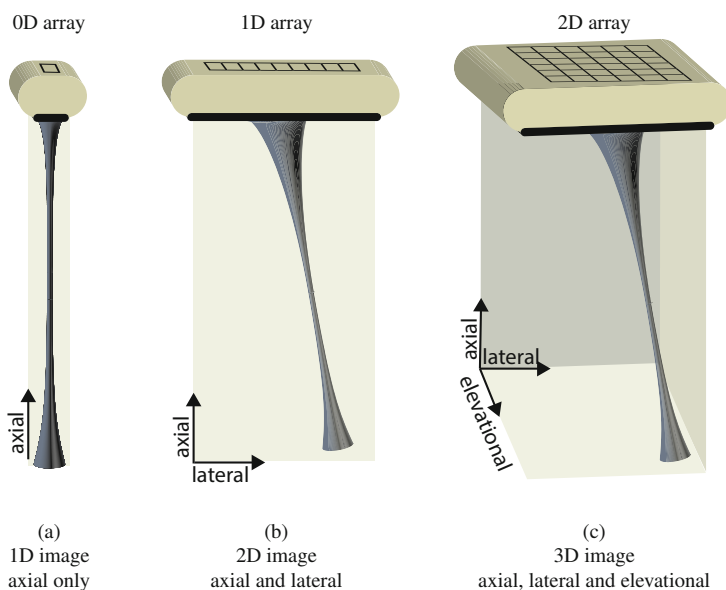


Fig. 1.8 Illustration of imaging in one or more dimensions. **(a)** A single ultrasound element can only image in 1 dimension. It can only resolve the axial (or radial) distance from the element if the speed of sound is known. **(b)** A one-dimensional array can use axial-lateral triangulation to image features in a single image plane. **(c)** A two-dimensional array can steer the ultrasound beam in lateral and elevational directions and thus image a 3D volume

two-dimensional imaging. Established, albeit very specialized, are single-element Doppler imaging devices for fetal heart rate, to be introduced and discussed later. Two-dimensional arrays exist as well and are mostly found in cardiology, though they are currently also entering the realm of abdominal imaging and other applications.

1.3.3 Resolution (Axial, Lateral, and Elevational)

Resolution is the measurement that determines what feature size can be imaged, i.e. resolved. Ultrasound beams have significant differences in their axial, lateral, and elevational resolution. The best resolution is achieved in the axial direction (Δx) and equals the product of the number of cycles in the transmit pulse (N) and the wavelength λ . Lateral resolution is proportional to the product of λ and the f -number ($f\#$). The latter is defined as the ratio of distance to the focus (F) divided by the lateral extent of the emitting aperture D_{lat} , i.e. F/D_{lat} . The elevational beam width is defined in the same way, except that the elevational aperture size must be used. A one-dimensional array has a fixed elevational aperture but a variable (electronic) lateral aperture. When imaging shallow features, only a small fraction of the aperture is active. When imaging a larger depth feature, the full aperture is active. Which part of the aperture is active is controlled by a constant $f\#$ approach. Typically an $f\#$ of 3 or 4 is used. For a focus at 2 cm depth, an aperture width of 5 mm ($f\# = 4$) is used. For a 10 MHz array ($\lambda = 154 \mu\text{m}$), this corresponds to approximately 32 elements. Assuming a transmit wave with one cycle ($N = 1$), the axial resolution is $154 \mu\text{m}$ (Eq. 1.9). For an $f\#$ of 4, the lateral resolution is $616 \mu\text{m}$. Assuming an elevational aperture of 2 mm yields a 1.54 mm elevational resolution.

$$\Delta x = N \cdot \lambda \quad \Delta y = \lambda \cdot \frac{F}{D_{lat}} \quad \Delta z = \lambda \cdot \frac{F}{D_{ele}} \quad (1.9)$$

1.3.4 Grating Lobes and Side Lobes

Beamforming using finite arrays creates grating and side lobes. These overlap with the main beam and produce clutter. Side lobes are generated due to the finite length of the used array. The elements at the ends, i.e. the first and last array element, have only one neighbor, whereas elements 2 to second-to-last have neighbors on both sides. This creates an imbalance in the transmitted wave, termed *side lobes*. *Grating lobes* originate from spacing array elements too far apart from each other. The relationship between the direction of existing side (θ_s) and grating lobes (θ_g) is given as

$$\begin{aligned} \theta_s &= \arcsin \frac{\lambda n}{a} \\ \theta_g &= \arcsin \frac{\lambda n}{p} \end{aligned} \quad (1.10)$$

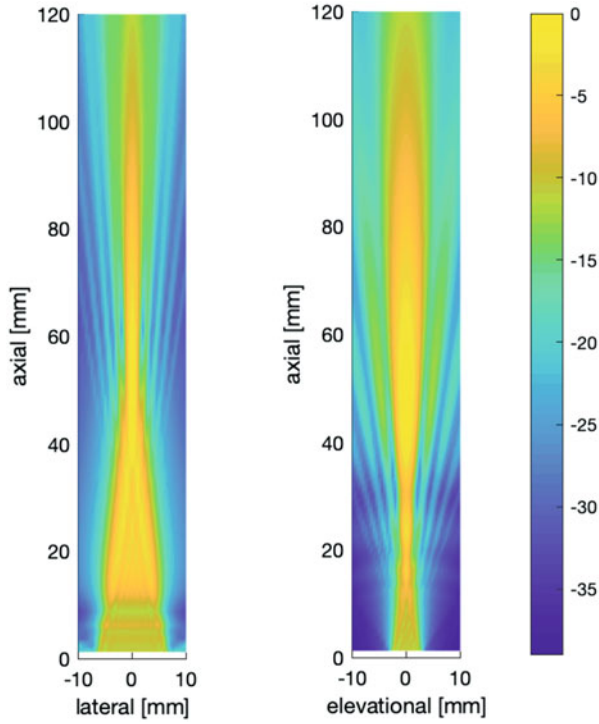


Fig. 1.9 Acoustic transmit pressure field plots of a linear array transducer (3.75 MHz center frequency). Left: Lateral-axial plane. Right: Elevational-axial plane (right). The lateral focus was set at 50 mm, whereas the elevational focus, given by the lens of the transducer, was 20 mm. The color bar shows the transmit pressure in dB relative to the maximum at 50 mm axially. Side lobes can be seen in symmetry to the main lobe. Note: The color bar is showing pressure in dB. Pressure fields computed using Field II [5]

where λ is the wavelength, n is the order of the side or grating lobe, a is the size of the aperture, and p is the pitch. Side lobes can be suppressed by driving edge elements at lower electric power. This is termed apodization. Here the aperture is driven non-uniformly using a tapering function, such as a Hamming window or other functions. Grating lobes are avoided by spacing array elements sufficiently close to each other. Linear arrays are spaced at λ and must not be steered more than approximately 20° to avoid grating lobes. Phased arrays are spaced at $\lambda/2$ and do not have a steering limitation.

An example of side lobes is shown in Figs. 1.9 and 1.10. The field of an array spaced at λ is shown, i.e. a linear array. As the beam is not steered, only side lobes are visible and no grating lobes. These could be suppressed using apodization. Techniques for such are presented in the textbook literature [6, 25, 26, 37].

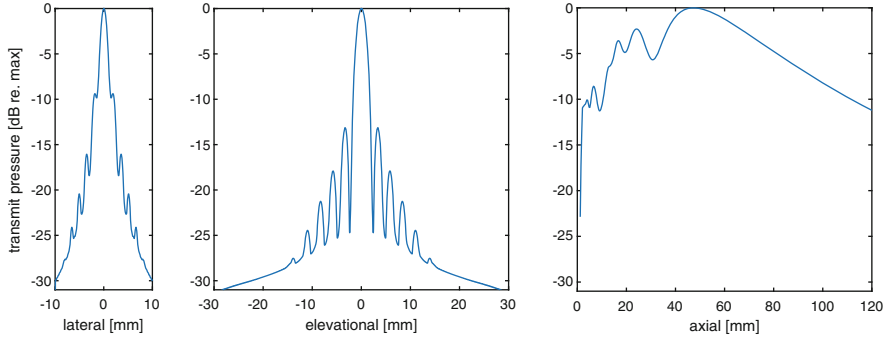


Fig. 1.10 Cross-sectional plots of the linear array transducer transmit pressure fields shown in Fig. 1.9. Left: Lateral beam profile through the axial focus. Middle: Elevational beam profile through the axial focus. Right: Axial beam profile. Maximum pressure at focus, i.e. at 47.1 mm. Pressure amplitudes are in logarithmic units, i.e. in dB, relative to the maximum in the field. Therefore all resulting pressures are negative and the maximum is zero. Acoustic pressures computed using Field II [5]

1.3.5 Penetration

Ultrasound waves attenuate as they travel. Frequency and medium dictate to what maximum depth one can image. Theoretically, a 10 MHz probe on a clinical ultrasound scanner with 120 dB dynamic range can image to a depth of $120 \text{ dB} = 2 \times 0.5 \text{ dB/MHz/cm} \times 10 \text{ MHz} \times d \text{ cm}$, therefore $d = 12 \text{ cm}$. However, many ultrasound scanners display an effective dynamic range for a given imaging application. A more realistic value would be a 70 dB dynamic range, for which the resulting image depth would be 7 cm. Even that may be too generous, but on the correct order of magnitude.

1.3.6 Ultrasonic Imaging Modes

1.3.6.1 B-Mode

Ultrasound images are commonly known as grayscale images. Formally they are called B-mode images. The letter “B” stands for brightness, which encodes the strength of the scattered or reflected wave. The example image in Fig. 1.11 was acquired using a linear array and a so-called *phantom* (CIRS Inc., model 040GSE). This is typically a container filled with a base material, either agar, some other type of gel, or rubber, and it is meant to mimic structures of the human body and concurrently allow for quality control of the ultrasound probe and system. The base material contains sub-wavelength scatterers to mimic such structures in human tissue. These produce the speckle pattern that is seen throughout the image. It is not noise, as can be easily observed, as the pattern does not change unless the probe moves. In fact, if the probe moves but returns to the same exact position, then the exact same, seemingly random, speckle pattern returns as well. The grayscale to

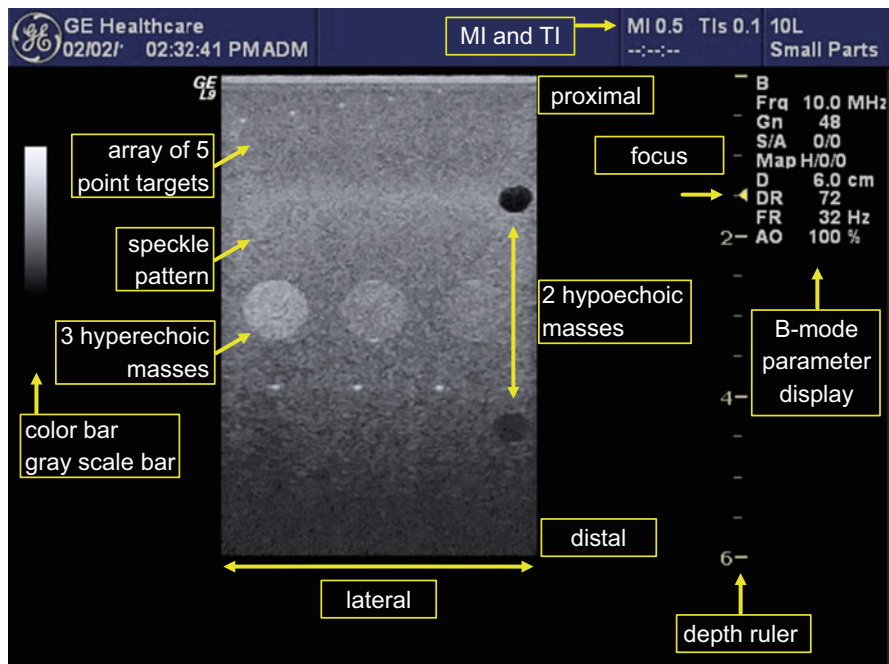


Fig. 1.11 Example of a B-mode ultrasound image, acquired using a linear array. B-mode is the most common imaging mode in ultrasound. It encodes scattering or reflecting structures in grayscale or brightness, hence B-mode. The annotations are elaborated on in the main text and in Table 1.3

physical intensity mapping is shown as the grayscale bar, commonly called a *color bar* on the left side of the image. It consists of 255 steps and can be a linear mapping or follow some kind of gamma correction or curve. Quantitative image analysis uses this information as it linearizes intensity. Several B-mode parameters are displayed on the screen. They are typically displayed in a section. Here the section starts with “B” indicating that the information relates to the B-mode. Other modes could be shown simultaneously, hence the label. Please refer to Table 1.3 for a discussion of these parameters. Most ultrasound images are shown with the probe located on the top of the image (proximal label). The field of view is 6 cm (distal label) as indicated by the depth ruler on the right. Zero centimeters is at the probe location. There is commonly no ruler for the lateral image extend. The authors know of only one exception to the probe being located on the top of the image, namely fetal echo, i.e. fetal cardiac ultrasound, where the image convention is upside down from the format shown here. It is possible that in the future manufacturers will allow for additional flexibility in image orientation. In dentistry it may be helpful, since intuitive, to position the probe on the left side of the image when obtaining a sagittal view of a tooth.

Table 1.3 Example listing of user controlled B-mode parameters on a diagnostic ultrasound scanner

Parameter	Definition
Frq	Center frequency of the transmitted beam, here 10 MHz
Gn	Receive gain the scanner applies to the acoustic echoes
S/A	Image filtering specific to this brand/model
Map	Mapping of physical wave intensities to display grayscale
D	Image depth
DR	Dynamic range, here 72 dB
FR	Frame rate, here 32 frames per second, 32 Hz
AO	Acoustic output, here 100%
MI	Mechanical index
TI	Thermal index, here for soft tissue (TIs), T1c stands for cranial bone and T1b for bone

User controllable parameters differ across scanner models and brands

While the overall ultrasound image is of lateral uniform brightness it can be observed that its axial brightness tapers off after approximately 4 cm depth. In fact there is a local enhancement across the lateral range at 1.5 cm depth. This is due to a user setting, the imaging focus. A yellow triangle can be found near the depth ruler. It indicates where the beamformer focuses the transmit beam. As can be seen in the image, the focused beam results in a brighter scatter from that depth. This is not because of the phantom but because of a stronger acoustic illumination at that depth. Not all ultrasound scanners allow the user to specify a focus location, but set it automatically. The system shown here is a GE Logiq 9 as branded on the top left side of the ultrasound image. This logo shows if the user swapped the ultrasound image left to right. Since most ultrasound probes can be held in reverse (with respect to left-right), scanners allow the user to flip the image left to right. If the image below was flipped, the logo would appear on the right.

Five types of phantom features can be observed in the ultrasound image. First the uniform background. Any broken piezoelectric elements in the ultrasound probe or broken signal channels in the ultrasound scanner could potentially produce a non-uniformity in the *lateral* direction of the image. On the very top of the image, within the first millimeter of the image is a bright line across the entire lateral width. This brightness is caused by the piezoelectric elements ringing down after their electric excitation, plus any reverberation of the launched acoustic waves within the matching layer and the elevational focus lens. The second feature is an array of five-point targets (100 μm diameter, actual nylon monofilaments oriented elevationally) at 1–5 mm away from the top end of the gel. Note that the imaging array reads approximately 2.2 mm to the first target. The difference of 1 mm may be the surface cover of the phantom. While 100 μm is not much smaller than the wavelength (here 154 μm), it is possible to measure the apparent axial and lateral extent of these filaments to obtain performance information of the ultrasound probe and scanner. While the filaments are 100 μm across, if the lateral resolution of the ultrasound

beam is $600\ \mu\text{m}$ (example from above), then the filaments diameter would image as $600\ \mu\text{m}$. In other words, for a known transmit frequency and focal distance, one can measure the lateral aperture size. The same holds for the axial measurement: for a known transmit frequency one can compute the number of transmit cycles in the acoustic wave.

Two hypoechoic cylinders (labeled as mass) are shown on the right side of the image. These are to evaluate clutter. Actual ultrasound beams are very complex. They not only point in the direction of the beamformer but also have side and grating lobes (discussed on Sect. 1.3.4). These extra lobes contribute to the received acoustic signal and cause hypoechoic areas to be filled to a certain degree. The top mass shows a stronger contrast to the background, i.e. is darker on the interior compared to the surrounding base material, than the lower mass that is filled with lighter gray pixels. This demonstrates that a sonographer might miss a mass or a lesion if it is filled with too much clutter signal. Three large cylinders are positioned across the image. Two of them have defined contrast compared to the background. The right two are +6 and +3 dB above background. The left cylinder is not specified. When performing quantitative image analysis these numbers can be tested for quality control. The bottom three-point targets can serve two purposes. First they are meant to calibrate the scanner for horizontal distance measurements. They are separated by 20 mm. Second, they demonstrate beam widening. While they are also $100\ \mu\text{m}$ in diameter, they appear significantly wider than those closer to the aperture, indicating a larger $f\#$ since the distance to the aperture increases and the aperture size may have reached its maximum size. In addition, the center frequency of the beam may have decreased at this depth due to frequency dependent attenuation, thus increasing λ and therefore the lateral resolution.

1.3.6.2 M-Mode

A major area of use for ultrasound is cardiac imaging, as ultrasound is a real-time modality and naturally able to image moving structures. B-mode can image at frame rates of up to 100 Hz on a radiological ultrasound scanner and up to 800 Hz on some cardiac scanners. While human hearts move significantly more slowly, rodent hearts can reach 600 bpm, i.e. 10 Hz. Extra sampling speed is required to temporarily resolve valve motion. Left ventricular wall motion of a Sprague Dawley rat is shown in Fig. 1.12. The top image is a sector scan B-mode image from a phased array typically used in cardiac imaging. The yellow dotted line in the image reaches from the probe aperture to the distal end of the field of view. This line marks the spatial part of the B-mode image that feeds into the M-mode image, which is shown on the bottom part of Fig. 1.12. The vertical axis of the M-mode is space. Here this space is 2 cm, shown on the left-side depth ruler of the B-mode image and the right side depth ruler of the M-mode image. One can see that the focus is set at 1.25 cm. The horizontal axis is time. In real-time this image continuously rolls from the right to the left. Note that zero time, i.e. now, is on the right. The left end of the time axis is $-1\ \text{s}$, i.e. there are approximately seven heart beats within one second, i.e. 420 bpm. In the M-mode image, the cardiac motion can be seen as contractions and dilations

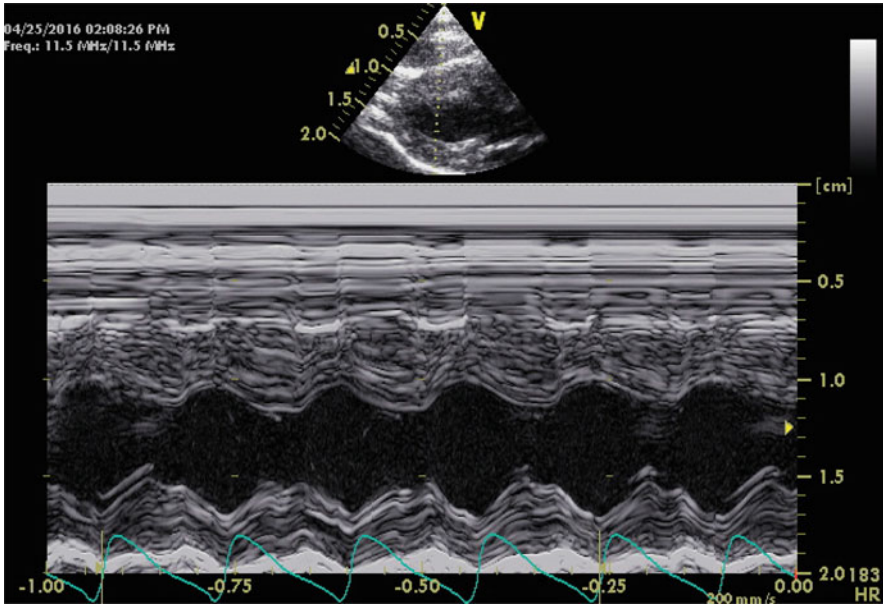


Fig. 1.12 Example of an M-mode ultrasound image. “M” stands for motion mode, and it is intended to display moving structures such as heart valves. As there are no inherent moving structures in dental imaging, its description is included as the reader may find a dental application of this mode

of the ventricle over time. The anterior and posterior walls move periodically in and outwards.

1.3.6.3 Extended View

Linear arrays have the smallest field of view (FOV), but the highest image quality. To extend the view, it is possible to enable a virtual convex view, which adds approximately 20° to each lateral side. Above it was mentioned that a linear array can steer the beam by up to 20° without compromise due to grating lobes. Another way to extend the FOV is to modify the ultrasonic probe, i.e. mount the elements on a curved housing, which is what a curvilinear array is. An alternative to that is the phased array, which also has a large FOV. However, both are still limited in the sense that they only capture the region in front of their aperture. To further extend the FOV, the ultrasound scanner allows the user to slide the probe laterally and track the changing image with real-time image correlation. This mode is essentially analogous to the panoramic image mode for digital photography. An MSK ultrasound, i.e. musculoskeletal ultrasound, example is given in Fig. 1.13.

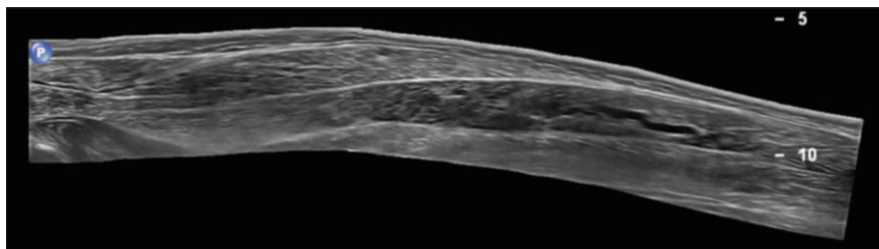


Fig. 1.13 Example of extended view of ultrasound image. This mode is analogous to the panoramic mode for digital photography. The ultrasound probe is moved laterally along the calf muscle. Following a significant curvature requires in-plane image correlation and image stitching. The scale can be derived from the depth indication on the right marking a 5 cm step

1.3.7 Blood Flow Imaging Modes

Ultrasonic blood flow imaging is based on methodologies that require the blood to be in motion. It is literally blood *flow* imaging, not imaging blood per se, but the movement of blood. In B-mode, blood appears hypoechoic, i.e. darker than the surrounding tissue. Blood consists of blood plasma and blood cells. The former does not contribute to ultrasound backscatter; the latter does.

1.3.7.1 Pulsed-Wave Doppler

Pulsed-Wave Doppler is the traditional blood flow imaging mode which is commonly known and produces real-time images as well as an audio signal. Though not conveyable in a book, the audio consists of the positive and negative velocity information of the pulsed-wave spectrum, transmitted through the left and right stereo audio speaker of the ultrasound system. Figure 1.14 shows the annotated screen interface of pulsed-wave Doppler, also known as PW Doppler, pulsed-wave, or as spectral Doppler. A B-mode image forms the central part of the display, where an additional line indicates where the spectral Doppler is obtained from. The line extends axially through the entire field of view and contains a gate with a short perpendicular line at the beginning and end of the gate. Within that gate the line is interrupted. Here is where the Doppler information is obtained. As shown in the example image, this part of the line should be positioned over the artery, vein, or as here, the lumen of the flow phantom. The length of the gate can be adjusted. Its current length is 8 mm and is shown as “SV” in the PW parameters section (see Fig. 1.14 and Table 1.4) towards the right of the PW section of the screen.

The PW display is similar to the M-mode display as it contains a horizontal time axis with zero on the right-hand side. Velocity is shown on the vertical axis, which is, in this example, shifted and inverted. The maximum is approximately -30 cm/s and the minimum $+10$ cm/s. Flow away from the transducer is shown as a positive velocity. A user control allows the axis to be flipped and negative velocities to be on the top. In addition, only negative velocities are present; for such, the baseline on the display can be shifted to use a larger range for negative velocities and a shorter

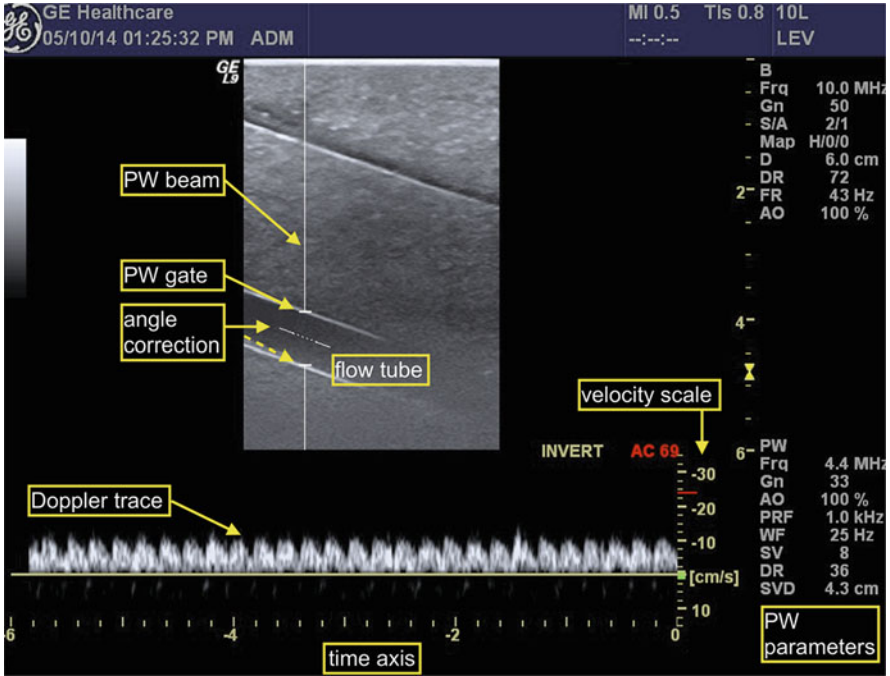


Fig. 1.14 Example of pulsed-wave (PW) Doppler imaging. PW-mode is used to display blood flow within a range gate as a function of time. The range gate is positioned within the accompanying live B-mode image. Annotations are elaborated on in the main text and in Table 1.4

Table 1.4 Example listing of user controlled PW-mode parameters on a diagnostic ultrasound scanner

Parameter	Definition
Frq	Center frequency of the transmitted beam, here 4.4 MHz
Gn	Receive gain the scanner applies to the acoustic echoes
AO	Acoustic output, here 100%
PRF	Pulse repetition frequency, here 1 kHz
WF	Wall filter, 25 Hz
SV	Sample volume, i.e. the length of the Doppler gate
DR	Dynamic range, here 36 dB
SVD	Sample volume depth, here 4.3 cm

User controllable parameters differ across scanner models and brands

range for positive ones. The Doppler equation governing the obtained velocities is

$$\Delta f = 2 \cdot f_0 \cdot \frac{v}{c} \cdot \cos(\alpha) \quad (1.11)$$

where Δf is the Doppler frequency shift for a transmitted wave with center frequency f_0 in a medium of speed of sound c , imaging an object moving with velocity v along a path with angle α with respect to the Doppler beam. The factor 2 is due to the fact that the scatterer is moving; hence it sees a Doppler shifted incoming wave and also becomes a moving source as it scatters the ultrasound. The angle α is shown as the dashed line on the center of the Doppler gate and its numerical value is shown as “AC” (angle correction) on the top right of the Doppler spectrum. In the example a 69° angle correction was dialed in. Angles that are too large ($>60^\circ$) produce beam artifacts that yield unreliable velocity information. For such angles the AC is displayed in red color, as in this example. For those cases the user should reposition the ultrasound probe to find a better acoustic path with a shallower angle. Changes in the AC will directly change the labels on the velocity axis. The Doppler spectrum itself will not change.

1.3.7.2 Color Flow/Power Mode

Color flow (CF) is a blood flow imaging mode in which flow is shown as color overlaid on the B-mode image. Red and blue pixels indicate flow towards and away from the transducer, respectively. Unlike PW Doppler, no temporary (past) information is shown, only real-time. A two-dimensional region of interest, called *color ROI*, is chosen in which color flow is acquired and displayed. Figure 1.15 shows an example with an angled (steered) color ROI, framed by a yellow beige line. A color bar replaces the B-mode gray scale bar and depicts the association between color and velocity. In the example, light blue indicates a velocity of $+10$ cm/s, whereas -10 cm/s corresponds to yellow. Both colors transition to 0 cm/s from the extremes. In the middle around 0 cm/s is a black-colored range, which represents the wall filter (WF), i.e. its velocity range spans from $-v_{WF}$ to $+v_{WF}$. In the example in Fig. 1.15 the WF is set to 103 Hz. Given a PRF and maximum velocity of 1.3 kHz and 10 cm/s, $v_{WF} = 10$ [cm/s] \times 103 [Hz]/1.3 [kHz] = 0.8 [cm/s].

The purpose of the wall filter is to literally remove signal originating from the lumen wall. A pulsatile lumen may contribute Doppler signals not only from the flowing blood but also from a pulsatile wall. As the lumen pressure changes throughout the cardiac cycle, the wall will displace. Two factors enhance the contribution of this motion to the Doppler processor. First the orientation: While blood most often moves at an angle with respect to the Doppler beam, the expanding or contracting wall moves directly to or from the transducer aperture, i.e. in-line with the Doppler beam. Hence its contribution to the Doppler signal is undiminished (angle α is zero, i.e. $\cos(\alpha) = 1$). Second, the wall is a very strong reflector. Compared to the blood cells, its signal is orders of magnitude larger, and it would dominate the Doppler processing chain. The wall filter removes velocities, i.e. frequencies, slower/smaller than the WF setting. There is a range of displays for the

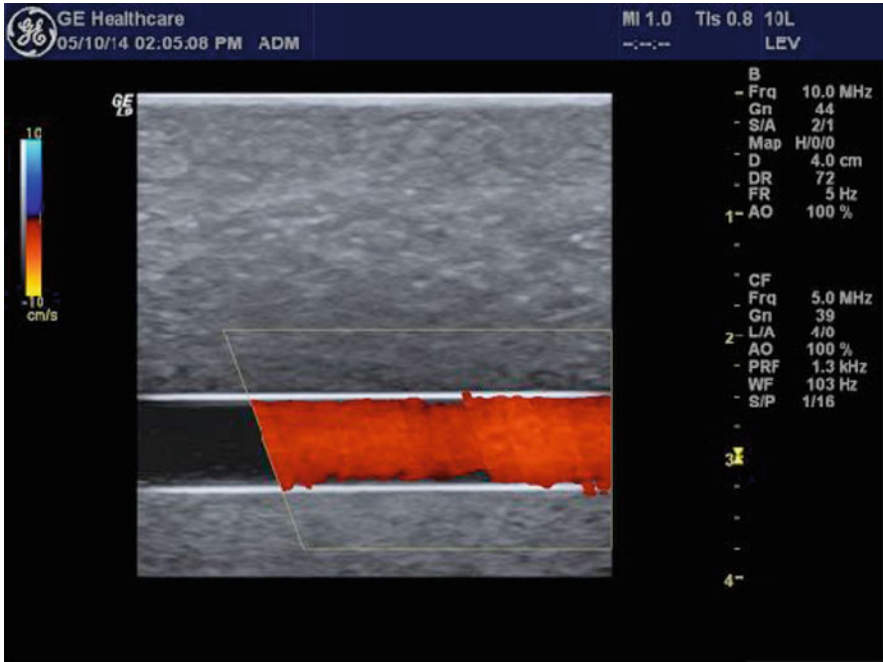


Fig. 1.15 Example of color flow imaging, which is used to display blood flow within the 2D B-mode image. For such, a color box is placed in the region of interest, i.e. across the lumen of interest. Within this box the ultrasound scanner detects temporal changes in the echoes and displays them as color pixel. In this example blue indicates blood moving towards the ultrasound probe and red moving away, as indicated by the color bar on the left. Since the lumen is parallel to the ultrasound probe, the color box is slanted to create an artificial angle and display blood flow parallel to the probe

WF, including straight frequency in Hz, or as a fraction of the maximum velocity or PRF, or qualitatively as low, medium, or high.

There are several parameters associated with color flow imaging. Some of them are listed in Table 1.5. *Packet size* is one of them: and it controls how many firings are averaged before they are displayed. In other words it controls quality but also responsiveness. A packet size of 8 will be able to update velocities twice as fast as a packet size of 16. As indicated in Fig. 1.15 the frame rate dropped to 5 Hz, as opposed to 43 Hz in the PW Doppler example in Fig. 1.14. Where PW Doppler only images one line, color flow images close to 50.

1.3.7.3 Aliasing

One of the most important parameters of flow imaging is the *pulse repetition frequency* (PRF). It controls how often the scanner transmits a beam to track the flow. A PRF that is too large will essentially transmit too often and waste resources, or even produce heating in the field of view. On the screen this is reflected as

Table 1.5 Example listing of user controlled color flow-mode parameters on a diagnostic ultrasound scanner

Parameter	Definition
Frq	Center frequency of the transmitted beam, here 5 MHz
Gn	Receive gain the scanner applies to the acoustic echoes
L/A	(Lateral) line density (4) and frame averaging (off)
AO	Acoustic output, here 100%
PRF	Pulse repetition frequency, here 1.3 kHz
WF	Wall filter, 103 Hz
S/P	Spatial filtering (1) and packet size (16)

User controllable parameters differ between scanner models and brands

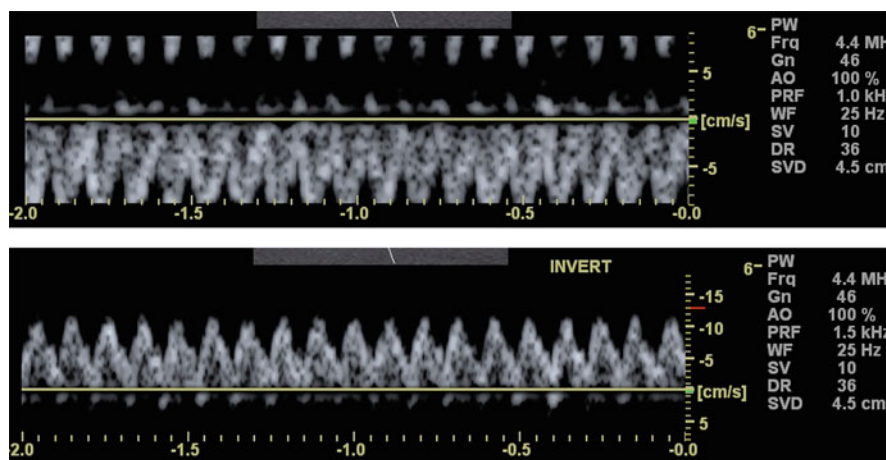


Fig. 1.16 Example of pulsed-wave Doppler aliasing. Aliasing occurs when a recording device is slower than the action being recorded. The reader may recall movies in which wheels of forward moving cars appear to be reversing. This is due to the frame rate of the camera being slower than the rotation of the wheels. If blood moves at a rate faster than the PW Doppler firings, i.e. the pulse repetition frequency (PRF), then flow aliases. This manifests itself as flow going to opposite direction. In the top panel, reverse flow at a maximum speed of 10 cm/s exceeds the display limit of 9 cm/s. This limit results from the PRF of 1 kHz. Flow beyond 9 cm/s is depicted as forward flow reaching from 9 to 8 cm/s, i.e. the flow waveform tops are clipping and display upside down from the top of the display. After increasing the PRF to 1.5 kHz and reversing the display, the waveform is no longer clipped

a mismatch between displayed velocity range and measured velocity range. In Fig. 1.14 the maximum flow velocity is approximately 10 cm/s, yet, the scale reaches up to 30+ cm/s. This range is too large; the PRF, here 1 kHz, could be reduced by a factor of 3 or more. A PRF that is too small will result in aliasing. Two scenarios are shown in Fig. 1.16. For a PRF of 1 kHz the imaged flow in the top panel aliases, i.e. its fastest velocities exceed the display range and wrap around to the opposite end of the range, here from maximum negative to maximum positive flow. There are three

steps to change the scanner configuration. First, increase the PRF to capture the flow more often, here to 1.5 kHz. Second, change the baseline to show a velocity range suitable for the observed flow, here approximately -5 to $+15$ cm/s. Third, invert the display to show systole on the top side of the PW display.

1.3.8 Advanced Image Modes

Ultrasonic imaging has evolved from simple delay-and-sum beamforming as described above to overcome economic and physical limitations to produce greater image detail and increase contrast.

1.3.8.1 Harmonic Imaging

Harmonic imaging is a method by which a wave with frequency f_0 (e.g., 5 MHz) is transmitted into the body and a wave with twice the frequency, i.e. $2 \times f_0$ (10 MHz), is expected back [38]. Two times f_0 is the first harmonic of f_0 , hence the name *harmonic imaging*.

Equation (1.1) introduced the linear wave equation. Sound at f_0 entering the body will be reflected and scattered at the same frequency. A nonlinear wave equation is needed to theoretically describe the creation of harmonics. Several solutions have been offered in the literature, including the Westervelt equation [39], the Burgers equation [40], and the KZK equation [41, 42]:

$$\frac{\partial^2 p}{\partial z \partial t} = \frac{c_0}{2} \nabla^2_{\perp} p + \frac{\delta}{2c_0^3} \frac{\partial^3 p}{\partial t^3} + \frac{\beta}{2\rho_0 c_0^3} \frac{\partial^2 p^2}{\partial t^2} \quad (1.12)$$

$$\beta = 1 + \frac{B}{2A}$$

While these theoretical descriptions exceed the scope of this book chapter, they can illustrate the complexity of the underlying formalism as well as the dependence on the biological medium (Table 1.6). Generally speaking, driving human tissue with sound pressures above 0.5 MPa results in harmonics [38]. Insonification at less than 0.5 MPa only returns the original frequency. While ultrasound scanners do not display information on the current sound pressure, they do display the mechanical index (MI). By use of Eq. (1.8) one can compute the rarefactional sound pressure from the MI and the transmit frequency.

Figure 1.17 shows the transmit receive beam profile of an ultrasound beam with $f_0 = 24$ MHz at f#4. The left panel shows the beam profile with a dynamic range of 36 dB, starting at 0 dB. In the focus at 10 mm, the beam's full width at half maximum is approximately $250 \mu\text{m}$. This size is suitable to image the interdental papilla (also termed interdental gingiva) soft tissue without interference from the adjacent teeth. However, the ultrasound beam is wider than $250 \mu\text{m}$ (as shown in the right-hand panel of Fig. 1.17) and even though the beam intensity drops significantly, the

Table 1.6 Listing of tissue parameters B/A for nonlinear sound propagation [30, 43]

Tissue	B/A
Blood	6.1
Brain	6.5
Fat	10
Liver	6.8
Muscle	7.4
Skin	7.8
Water	5.2

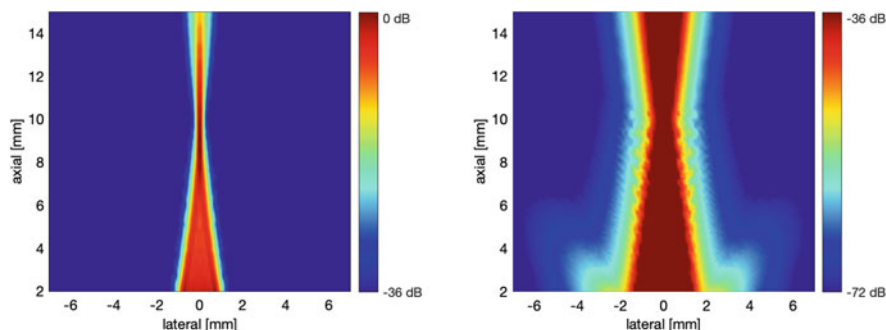


Fig. 1.17 Objective for harmonic imaging. Imaging is based on beamforming to locate the scattering structures that contribute to the receive signal. Left: The first 36 dB (i.e., -36 to 0 dB) of the imaging beam simulated here are fairly confined to a tight beam for good lateral spatial resolution in the focus at 10 mm axially. Right: The next 36 dB, i.e. -72 to -36 dB, are contributing lateral components, spreading the beam considerably. At the 10 mm focus the -36 dB beam is 4 to $5\times$ wider than the full width at half maximum (~ 250 μm). Any strongly reflecting structures would contribute clutter signal to the ROI in the center of the beam. Driving the transmit beam at high sound pressure generates nonlinear tissue scattering. This nonlinearity transforms an incoming wave at f_0 to a scattered wave at $2 \times f_0$. Using frequency filtering can remove the linear scattering clutter signals

scattering or reflecting objects, i.e. the adjacent teeth, have a much larger reflection coefficient than soft tissue. This causes what is known as clutter, i.e. off-beam contributions to the receive signal that shadow on-beam structures. By driving the ultrasound transducer at higher sound pressure the central part of the beam causes the illuminated soft tissue to scatter $2 \times f_0$, which can be filtered out from the receive signal. Therefore, off-beam clutter contributions at f_0 can be removed by frequency filtering. Figure 1.18 shows example images for two traditional cases where the same frequency is used for transmit and receive and one case where harmonic imaging is used, i.e. the transmit is a $f_0 = 12$ MHz and the receive signal is filtered to remove f_0 and only allow $2 \times f_0 = 24$ MHz. The harmonic imaging case shows less fill-in of hypoechoic structures than the straight f_0 cases.

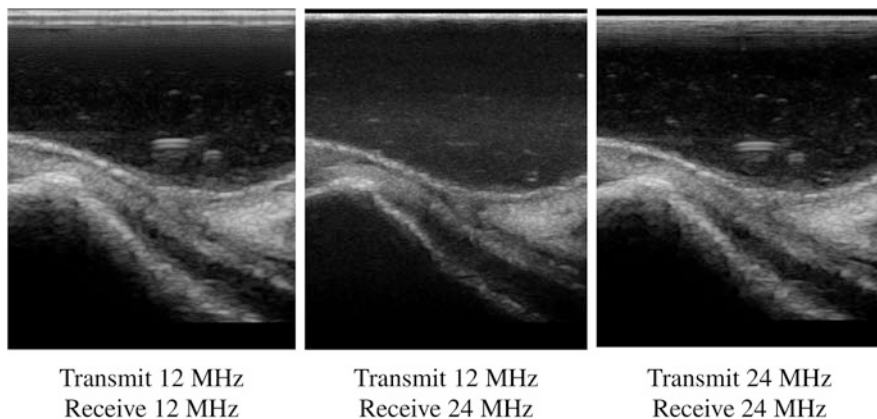


Fig. 1.18 Three examples of harmonic imaging. The same oral structure was imaged three times, with varying transmit (TX) and receive (RX) frequencies. In general higher frequencies produce better spatial resolution and better contrast unless penetration is limited. Left and right sides show the cases where TX and RX are at the same frequency, 12 and 24 MHz, respectively. The latter shows better delineation than the former. However, the middle case with TX at 12 MHz and RX at 24 MHz shows less clutter than the right side. Hypochoic regions are more pronounced and less filled with clutter

1.3.8.2 Image Compounding

Ultrasound images of specular reflectors suffer from lack of signal at essentially non-perpendicular insonification angles. In other words, when an ultrasound beam impinges on a reflecting surface at an angle other than 90° , then the beam is reflected away from the receiving transducer and is thus not recorded. The result is no signal, a hypochoic region. This is the case for blood vessels, bones, roots, implants, abutments, etc. A possible solution is to vary the image angle and combine images from a range of angles. This method is called *spatial compounding* and is illustrated in Fig. 1.19.

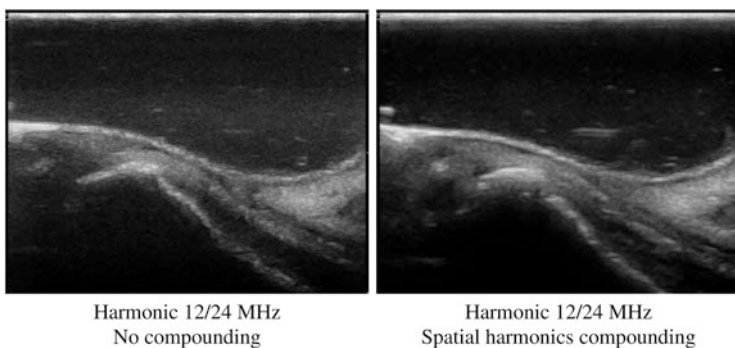


Fig. 1.19 Examples of spatial image compounding. Underlying imaging is harmonic imaging with a 12/24 MHz pair. Right side is (spatial harmonics) compounded, left side is not. Compounding enhances spatial delineation

1.4 Artifacts

Ultrasonic imaging artifacts can be multifactorial and their manifestations in diagnostic imaging are well documented in the literature. General artifacts discussion and classifications are given by Prabhu et al. [44], Hindi et al. [45], Scanlan [46], Kirberger [47], Park et al. [48], and Feldman et al. [49], as well as Kremkau and Taylor [50]. Reverberations and comet tail artifacts, as are visible in dental ultrasound, are discussed in particular by Lichtenstein et al. [51]. Slice-thickness artifacts are discussed by Goldstein and Madrazo [52]. Three-dimensional ultrasound artifacts are addressed by Nelson et al. [53]. Color flow and spectral Doppler artifacts are discussed by Jenssen et al. [54]. Improving images that suffer from artifacts is the topic of a review by Ortiz et al. [55]. Examples of image artifacts are presented in the following subchapters.

1.4.1 Coupling, Shadowing, and Enhancement

Sound propagation relies on the ambient acoustic impedance Z and speed of sound c to be in a range typical for medical imaging, i.e. $Z = 1.54 \text{ MRayl}$, $c = 1540 \text{ m/s}$. Placing an ultrasound transducer on the skin without using ultrasound coupling gel or similar will prevent the sound from penetrating the skin, as the majority of the sound energy is reflected on the air gap between the transducer aperture and the skin. The speed of sound in air is 340 m/s and its acoustic impedance is $Z = 0.0034 \text{ MRayl}$. Figure 1.20, left panel, illustrates the effect of poor coupling. Part of the left side aperture is not correctly coupled to the imaged phantom. Shadowing is an artifact where a strong reflector causes a significant reduction of the forward-propagating acoustic wave, which manifests itself as an artifactually hypochoic tissue region (middle panel). Enhancement is the opposite effect. Here a lower background reflector or scatterer yields a forward-propagating acoustic wave that then manifests itself as an artifactually hyperechoic tissue region (right panel).

1.4.2 Refraction

Analogous to optics, ultrasound beams are refracted when they transverse from medium 1 with speed of sound c_1 to medium 2 with speed of sound c_2 [56]. This is known as Snell's Law, where the ratio of c_1/c_2 equals the ratio of $\sin(\alpha_1)/\sin(\alpha_2)$, where α_1 is the incident beam angle with respect to the interfacial surface and α_2 is the refracted beam angle. Ultrasound imaging systems assume a constant speed of sound of $c = 1540 \text{ m/s}$. Using that speed c , the system maps temporal information t from receiving beam information to spatial coordinates ($s = c \times t$). Figure 1.21 shows simulation and imaging examples of beam refraction [57]. In the simulation (left panel) a sound beam travels upwards through ultrasound gel (medium ①) towards a human skin interface (double parallel curved lines, medium ②). Due to

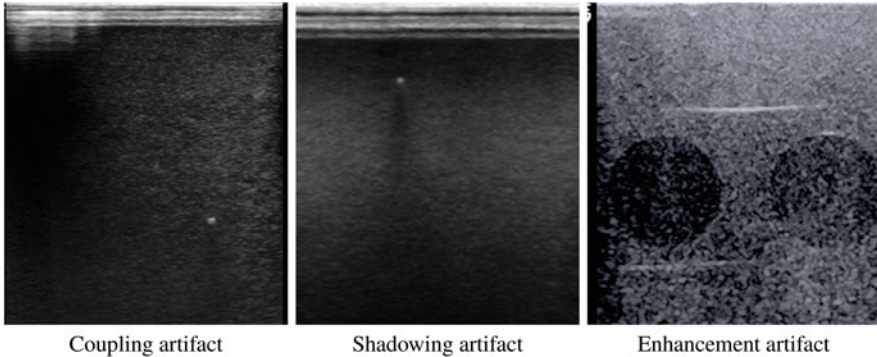


Fig. 1.20 Examples of image artifacts. Left panel: Effect of poor coupling. Ultrasound coupling gel is applied to the center and the right side of the aperture. The sound emitted on the left side of the aperture is reflected by the air gap between the aperture and the surface of the imaged ultrasound phantom. Middle panel: A point target comprised of a $100\ \mu\text{m}$, nylon monofilament is imaged in cross-section. Its acoustic impedance differs from the surrounding host material and causes a strong specular reflection. The reflected acoustic energy diminishes the forward going wave and thus casts a shadow distal to the point target. Right panel: Hypochoic regions can produce enhancement on their distal side as the penetrating sound wave does not *lose* as much energy, i.e. the backscattered energy from the hypochoic region is less from than the surrounding tissue. The image shows two hypochoic cylinders in cross-section. Their distal region is enhanced, whereas the background tissue in-between the cylinders appears darker

the shallow incidence angle between the beam and the skin surface, the incident beam is split into two beams, one refracted and one reflected. The refracted beam leaves a shadow region behind the skin in medium ③. Without the speed of sound changes between the three media, the incident beam would travel straight, whereas here the beam is split. A clinical example is shown in Fig. 1.21 (right panel), i.e. an ultrasound scan of breast tissue. The incident beam also enters the field of view from the bottom. The bright curved 45° -oriented line is the skin surface. This setting is analogous to the simulation in the left panel. There is a shadow region due to beam refraction, which is circled in blue. Clinically this shadow is covering a region which is prone to cancers. Health-care providers need to recognize this artifact and find ways to circumvent the image degradation to adequately support their medical assessment.

1.4.3 Noise

Noise is always a part of any signal. Every ultrasound image contains noise. However, in most meaningful diagnostic images, the noise has a much smaller amplitude than the remaining signal, i.e. the signal to noise ratio, as known as SNR, is high. Figure 1.22a shows a case with poor system choices. A high frequency probe with a shallow elevational, i.e. fixed focus, lens is set up to image relatively deep in an attenuating phantom, here 2.5 cm and 0.5 dB/MHz/cm, which is deep for

this combination of lens, frequency, and phantom. The result is image noise. A still image cannot convey how image noise appears on the screen. Speckle “noise” is the typical ultrasound image granularity. It does not change over time, only when the ultrasound probe moves. Non-speckle, electronic, traditional noise changes over time. For an ultrasound probe remaining at exactly the same spatial position over time, the image portion that contains noise will fluctuate. This fluctuation is the best indicator for image noise. Typically noise appears in the image beginning from the distal side, progressing to the proximal side, since the ultrasound wave diminishes over space.

1.4.4 Mirroring

Mirror artifacts are not uncommon in the human body. They occur when the ultrasound beam or the scattered signal is reflected by a finite surface (see Fig. 1.22b). This can include bones, implants, and gas interfaces, such as the lung (diaphragm), stomach, intestine, etc. The user can challenge mirror image appearances by changing the probe position and reevaluating the image.

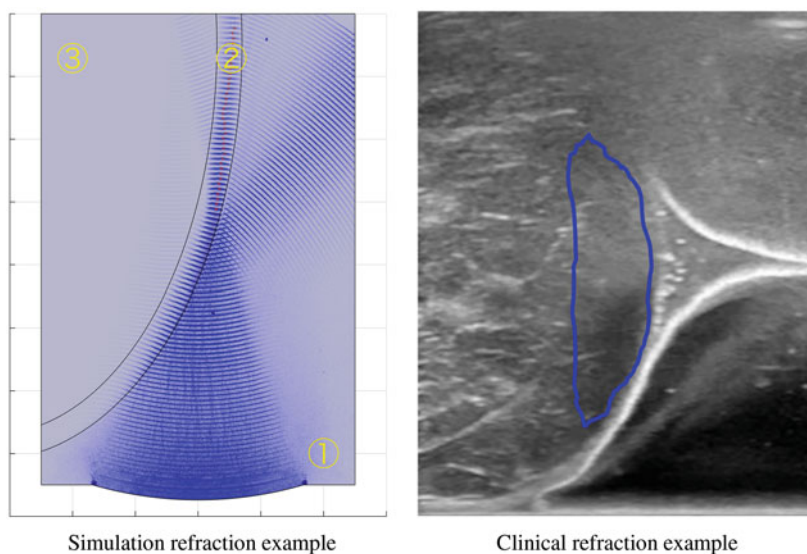


Fig. 1.21 Examples of refraction image artifacts. Left panel: Simulation of an acoustic beam emerging from the bottom, traveling through ultrasound coupling gel (medium ①) and being refracted to the right by the curved skin surface (medium ②) into breast tissue (medium ③) [57]. Right panel: Clinical refraction example of a hypoechoic region below the skin surface [57]

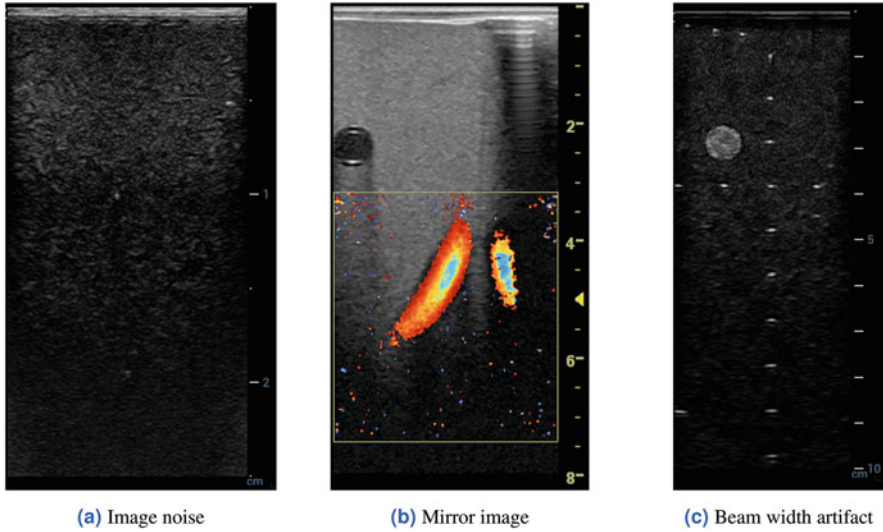


Fig. 1.22 Examples of image artifacts. **(a)** Example of image noise. The displayed image is from a 24 MHz transmit with a 7 mm elevational focus, yet the image depth is 2.5 cm. At this high frequency and shallow elevational focus, it is not possible to obtain an image at this great depth. The result is noise. **(b)** Example of mirror image. The displayed image shows color flow visualizing a flow tube in a phantom. The right-hand side of the image is not fully coupled as can be seen from the right-side aperture. However, there are two flow tubes in the images, whereas the phantom contains only one. Moreover, the two lumens appear to be in part symmetric to each other. The right-hand lumen is truncated compared to its left side counterpart. It is produced by ultrasound beams being reflected from the right-hand housing wall of the phantom, thus producing a mirror image. **(c)** Example of beam width artifacts. The displayed image demonstrates how lateral resolution decreases with depth. The shown axial wire targets are all of the same physical size yet appear larger as depth increases. This is due to the decreasing lateral resolution of the ultrasound beam as it penetrates deeper tissues

1.4.5 Beam Width

Ultrasonic beams are shaped with electronic and mechanical lenses. The beam-former uses electronic delays to focus the beam and a certain aperture size to create an intended beam width. For 1D arrays the fixed-focus elevational lens on the transducer shapes the beam depending on the application of the probe. It can be for superficial imaging of teeth or peripheral blood vessels or for deep imaging, such as abdominal imaging. The beam width is minimal in the focal region and widens as it progresses beyond that spatial point. Figure 1.22c shows a 10 cm field of view in a phantom for spatial calibrations. The beam width can be estimated and measured by examining the apparent width of the (axial) wire targets. This width increases with depth and can be explained with Eq. (1.9), where the lateral beam width is related to the frequency and the $f\#$. Since $f\#$ is defined as focal length F divided by the aperture width D , i.e. $f\# = F/D$, it is obvious that at the point where the aperture

cannot widen more yet the focal length increases, the beam width has to increase as well. This is the case in Fig. 1.22c. It is also possible that the actual frequency of the acoustic wave decreases and thus the wavelength increases, but that is beyond the scope of this chapter.

1.4.6 Reverberation and Comet Tail Artifacts

Ultrasonic imaging assumes a continuously forward-propagating wave and speckle scattering from the penetrated tissue. However, some tissue structures or foreign body inclusions may change the acoustic path. Figure 1.23 left shows reverberation artifacts within a crown. The speed of sound and mass density of teeth are greater than those of soft tissue. In addition, the distal side of the crown is exposed to air, whose speed of sound and mass density are significantly lower than soft tissue. Therefore, the proximal and distal interface of the crown trap a certain amount of the incident sound wave and cause it to reflect within the crown multiple times, each time with diminishing energy. The ultrasound scanner associates the time of any received acoustic wave relative to the time when the original beam was transmitted and computes the distance of an associated structure based on the assumed speed of sound of 1540 m/s. As a result, the reverberating sound within the crown is interpreted as a structure that is equally spaced and distal to the front surface of the crown. Distinct parallel lines are visible when the front and back side of the underlying structure are parallel as well (left panel in Fig. 1.23). Any appreciable

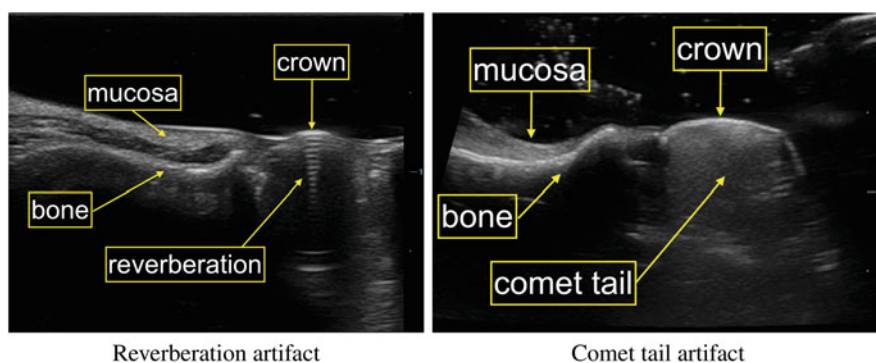


Fig. 1.23 Example of reverberation and comet tail artifacts. Sound, much like any wave, is reflected when it encounters an impedance change. In dental ultrasound the wave is reflected on bones, crowns, roots, implants, and others. For structures with parallel boundaries, crowns, and implants, for example, the sound can reverberate (left image) within them and slowly “leak” out towards both parallel boundaries. The sound “leaking” towards the ultrasound probe is received and displayed as a structure in the axial direction. Reverberating waves where individual reflections blend into a continuous wave, right image, are called *comet tail* or *vail* artifact

curvature, with respect to the acoustic wavelength in the structure, causes a diffuse reverberation, which is termed a *comet tail* or *vail artifact* (right panel in Fig. 1.23).

References

1. Gholizadeh S. A review of non-destructive testing methods of composite materials. *Proc Struct Integr.* 2016;1:50–7. ISSN: 2452-3216.
2. Drinkwater BW, Wilcox PD. Ultrasonic arrays for non-destructive evaluation: a review. *NDT E Int.* 2006;39(7):525–41. ISSN:0963–8695.
3. Hunter AJ, Drinkwater BW, Wilcox PD. Autofocusing ultrasonic imagery for non-destructive testing and evaluation of specimens with complicated geometries. *NDT E Int.* 2010;43(2):78–85. ISSN: 0963-8695.
4. Jenderka K-V, Koch C. Investigation of spatial distribution of sound field parameters in ultrasound cleaning baths under the influence of cavitation. *Ultrasonics.* 2006;44:e401–6. ISSN: 0041-624X.
5. Jensen JA. Field: a program for simulating ultrasound systems. In: 10th Nordic-Baltic conference on biomedical imaging published in medical & biological engineering & computing. Vol. 34, Issue: 1; 1996. p. 351–53.
6. Szabo TL. *Diagnostic ultrasound imaging: inside out.* London: Academic Press; 2004. ISBN: 0126801452.
7. Saini K, Dewal ML, Rohit M. Ultrasound imaging and image segmentation in the area of ultrasound: a review. *Int J Adv Sci Technol.* 2010;24.
8. Fenster A, Downey DB. 3-D ultrasound imaging: a review. *IEEE Eng Med Biol Mag.* 1996;15(6):41–51. ISSN: 0739-5175.
9. McGahan JP, Goldberg BB. *Diagnostic ultrasound.* Vol. 1. London: Informa Health Care; 2008. ISBN: 1420069780.
10. Caskey CF, Hu XW, Ferrara KW. Leveraging the power of ultrasound for therapeutic design and optimization. *J Control Release.* 2011;156(3):297–306. ISSN: 0168-3659. <https://doi.org/10.1016/j.jconrel.2011.07032>. %3CGo%20to%20ISI%3E://WOS:000298555000004.
11. Hynynen K. Focused ultrasound for blood-brain disruption and delivery of therapeutic molecules into the brain. In: *Expert Opin Drug Deliv.* 2007;4(1):27–35. ISSN: 1742-5247. <https://doi.org/1.1517/1742524741.27>. %3CGo%20to%20ISI%3E://WOS:000252825100004.
12. Bailey MR, et al. Physical mechanisms of the therapeutic effect of ultrasound (a review). *Acoust Phys.* 2003;49(4):369–88. ISSN: 1063-7710. <https://doi.org/10.1134/1.1591291>. %3CGo%20to%20ISI%3E://WOS:000184769300001.
13. Baker KG, Robertson VJ, Duck FA. A review of therapeutic ultrasound: biophysical effects. *Phys Ther.* 2001;81(7):1351–8. ISSN: 0031-9023. <https://doi.org/10.1093/ptj/81.7.1351>. %3CGo%20to%20ISI%3E://WOS:000169684600007.
14. Jiang XX, et al. A review of low-intensity pulsed ultrasound for therapeutic applications. *IEEE Trans Biomed Eng.* 2019;66(10):2704–18. ISSN: 0018-9294. <https://doi.org/10.1109/tbme.2018.2889669> %3CGo%20to%20ISI%3E://WOS:000487192000001.
15. Gorick, CM, Chappell, JC, Price, RJ. Applications of ultrasound to stimulate therapeutic revascularization. *Int. J. Mol. Sci.* 2019;20(12):3081. ISSN: 1422-0067. <https://doi.org/10.3390/ijms20123081>. %3CGo%20to%20ISI%3E://WOS:000473756000231.
16. O'Reilly MA, Hynynen, K. Emerging non-cancer applications of therapeutic ultrasound. *Int J Hyperthermia.* 2015;31(3):310–8. ISSN: 0265-6736. <https://doi.org/10.3109/02656736.2015.1004375>. %3CGo%20to%20ISI%3E://WOS:000355926300012.
17. Ebbini ES, Ter Haar, G. Ultrasound-guided therapeutic focused ultrasound: current status and future directions. *Int J Hyperthermia.* 2015;31(2):77–89. ISSN: 0265-6736. <https://doi.org/10.3109/02656736.2014.995238>. %3CGo%20to%20ISI%3E://WOS:000353167300002.
18. Miller DL, et al. Overview of therapeutic ultrasound applications and safety considerations. *J Ultrasound Med.* 2012;31(4):623–34. ISSN: 0278-4297. <https://doi.org/10.7863/jum.2012.31>.

- 4.623. %3CGo%20to%20ISI%3E://WOS:000302446100014.
19. Wells PNT. A range-gated ultrasonic Doppler system. *Med Biol Eng.* 1969;7(6):641–52. ISSN: 0025-696X.
 20. Lawson G, Dawes GS, Redman CWG. A comparison of two fetal heart rate ultrasound detector systems. *Am J Obstet Gynecol.* 1982;143(7):840–2. ISSN: 0002-9378.
 21. Kurjak A, et al. How useful is 3D and 4D ultrasound in perinatal medicine? *J Perinatal Med.* 2007;35(1):10–27. ISSN: 1619-3997.
 22. Yagel S, et al. 3D and 4D ultrasound in fetal cardiac scanning: a new look at the fetal heart. *Ultrasound Obstet Gynecol.* 2007;29(1):81–95. ISSN: 0960-7692.
 23. Barnett SB, Maulik, D. Guidelines and recommendations for safe use of Doppler ultrasound in perinatal applications. *J Matern Fetal Med.* 2001;10(2):75–84. ISSN: 1057-0802.
 24. Barnett SB, et al. International recommendations and guidelines for the safe use of diagnostic ultrasound in medicine. *Ultrasound Med Biol.* 2000;26(3):355–66. ISSN: 0301-5629.
 25. Morse PM, Ingard KU. *Theoretical acoustics.* Princeton: Princeton University Press; 1986. ISBN: 0691024014.
 26. Cobbold RSC. *Foundations of biomedical ultrasound.* Oxford: Oxford University Press; 2006. ISBN: 0199775125.
 27. Kinsler LE, et al. *Fundamentals of acoustics.* In: Kinsler LE, Frey AR, Coppens AB, Sanders JV, editors. *Fundamentals of acoustics.* 4th ed. Weinheim: Wiley-VCH; 1999, p. 560. ISBN 0-471-84789-5.
 28. Azhari, H. *Basics of biomedical ultrasound for engineers.* London: Wiley; 2010. ISBN: 0470561467.
 29. Hoskins PR, Martin K, Thrush, A. *Diagnostic ultrasound: physics and equipment.* Cambridge: Cambridge University Press; 2010. ISBN: 1139488902.
 30. Duck, FA. *Physical properties of tissues: a comprehensive reference book.* London: Academic Press; 2013. ISBN: 1483288420.
 31. Herring N, Paterson DJ. *Levick's introduction to cardiovascular physiology.* Boca Raton: CRC Press; 2018.
 32. Chivers RC, Hill, CR. Ultrasonic attenuation in human tissue. *Ultrasound Med Biol.* 1975;2(1):25–9.
 33. Barootchi S, et al. Ultrasonographic characterization of lingual structures pertinent to oral, periodontal and implant surgery. *Clin Oral Implants Res.* 2020;31(4):352–9.
 34. Branham ML, et al. Effect of ultrasound-facilitated fixation on oral mucosa density and morphology. *Biotech Histochem.* 2012;87(5):331–9.
 35. Hosokawa A, Otani T. Ultrasonic wave propagation in bovine cancellous bone. *J Acoust Soc Am.* 1997;101(1):558–62.
 36. Bond LJ, Chiang C-H, Fortunko CM. Absorption of ultrasonic waves in air at high frequencies (10–20 MHz). *J Acoust Soc Am.* 1992;92(4):2006–15.
 37. Schmerr LW Jr. *Fundamentals of ultrasonic phased arrays.* Vol. 215. Berlin: Springer; 2014.
 38. Anvari A, Forsberg F, Samir AE. A primer on the physical principles of tissue harmonic imaging. *RadioGraphics.* 2015;35(7):1955–64.
 39. Shevchenko I, Kaltenbacher, B. Absorbing boundary conditions for nonlinear acoustics: the Westervelt equation. *J Comput Phys.* 2015;302:200–21.
 40. Hamilton MF, Blackstock DT, et al. *Nonlinear acoustics.* Vol. 237. San Diego: Academic Press; 1998.
 41. Rozanova, A. The Khokhlov–Zabolotskaya–Kuznetsov equation. *C R Math.* 2007;344(5):337–42.
 42. Pinton GF, et al. A heterogeneous nonlinear attenuating full-wave model of ultrasound. *IEEE Trans Ultrason Ferroelectr Freq Control.* 2009;56(3):474–88.
 43. Wells PNT. Ultrasonic imaging of the human body. *Rep Prog Phys.* 1999;62(5):671.
 44. Prabhu SJ, et al. Ultrasound artifacts: classification, applied physics with illustrations, and imaging appearances. *Ultrasound Q.* 2014;30(2):145–57.
 45. Hindi A, Peterson C, Barr, RG. Artifacts in diagnostic ultrasound. *Rep Med Imaging.* 2013;6:29–48.

46. Scanlan KA. Sonographic artifacts and their origins. *Am J Roentgenol.* 1991;156(6):1267–72. ISSN: 0361-803X.
47. Kirberger RM. Imaging artifacts in diagnostic ultrasound—a review. *Vet Radiol Ultrasound.* 1995;36(4):297–306. ISSN: 1058-8183.
48. Park RD, et al. B-mode gray-scale ultrasound: imaging artifacts and interpretation principles. *Vet Radiol.* 1981;22(5):204–10. ISSN: 0196-3627.
49. Feldman MK, Katyal S, Blackwood MS. US artifacts. *RadioGraphics.* 2009; 29(4):1179–89. ISSN: 0271-5333.
50. Kremkau FW, Taylor KJ. Artifacts in ultrasound imaging. *J Ultrasound Med.* 1986;5(4):227–37. ISSN: 1550-9613.
51. Lichtenstein D, et al. The comet-tail artifact: an ultrasound sign ruling out pneumothorax. *Intensive Care Med.* 1999;25(4):383–8. ISSN: 0342-4642.
52. Goldstein A, Madrazo BL. Slice-thickness artifacts in gray-scale ultrasound. *J Clin Ultrasound.* 1981;9(7):365–75. ISSN: 0091-2751.
53. Nelson TR, et al. Sources and impact of artifacts on clinical three dimensional ultrasound imaging. *Ultrasound Obstet Gynecol.* 2000;16(4):374–83. ISSN: 0960-7692.
54. Jenssen C, et al. Ultrasound artifacts and their diagnostic significance in internal medicine and gastroenterology—part 2: color and spectral Doppler artifacts. *Z Gastroenterol.* 2016;54(6):569–78. ISSN: 0044-2771.
55. Ortiz SHC, Chiu T, Fox, MD. Ultrasound image enhancement: a review. *Biomed Signal Process Control.* 2012;7(5):419–28. ISSN: 1746-8094.
56. Sommer FG, Filly RA, Minton, MJ. Acoustic shadowing due to refractive and reflective effects. *Am J Roentgenol.* 1979;132(6):973–9. ISSN: 0361-803X.
57. Jintamethasawat R, et al. Acoustic beam anomalies in automated breast imaging. *J Med Imaging (Bellingham).* 4(4):045001. ISSN: 2329-4302 (Print) 2329-4302 (Linking). <https://doi.org/10.1117/1.JMI.4.4.045001>. <https://www.ncbi.nlm.nih.gov/pubmed/29057289>.